Functionalisation of MoS_2 2D layers with diarylethene molecules

†Marc Morant-Giner,[a] †José Miguel Carbonell-Vilar,[a] Marta Viciano-Chumillas,[a,*] Alicia Forment-Aliaga,[a,*] Joan Cano,[a] Eugenio Coronado[a]

Instituto de Ciencia Molecular, Universitat de València, C/Catedrático José Beltrán 2, 46980 Paterna, Spain. e-mails: alicia.forment@uv.es; marta.viciano@uv.es

† Equally contributed.

Functionalisation of two dimensional (2D) materials with stimuli-responsive molecules has been scarcely investigated. Here, MoS_2 layers obtained by chemical exfoliation are covalently and non-covalently functionalised using two photoswitchable diarylethene derivatives under their open- and closed-ring isomers. The choice of these light-responsive molecules is based on their excellent thermal irreversibility and fatigue resistance. The characterisation of the resultant molecular/2D heterostructures proves the successful anchoring of the molecules by both approaches as well as the influence that the driving interaction has in the photoswitching behaviour of the diarylethene isomers after their deposition on the 2D layer.

Introduction

2D materials have attracted great attention in the last years due to the emergent properties arising from the confinement of electrons in two dimensions and to their high surface-area-to-volume ratios, which render these materials attractive chemical and physical properties.[1,2]

Among 2D materials, an interesting family is that provided by layered transition metal dichalcogenides (TMDCs) with the chemical formula of MX_2 (M: transition metal, usually from groups IV-VII and X: chalcogen S, Se, or Te). Its structure consists of vertically stacked X-M-X slabs hold together by weak van der Waals interactions. This structure permits an easy exfoliation into ultrathin MX_2 layers by mechanical and chemical methods. TMDCs, and particularly MoS_2, have become a hot topic in materials science because of their applications in electronics,[3] optoelectronics,[4,5] sensing,[6,7] energy storage[8], photovoltaic devices[7] and catalysis.[9,10]

The most common MoS_2 polytypes are 2H and 1T, the former being the thermodynamically stable phase, with hexagonal structural symmetry and semiconducting properties, while the latter is a metastable phase with tetragonal structure and metallic behaviour.[11] Interestingly, molecules can tailor the MoS_2 properties by surface modification, expanding the possible applications for this 2D material.[12–15] Molecular approaches exploiting non-covalent forces via physisorption on MoS_2 have been developed.[12,16,17] Although these forces including electrostatic and van der Waals interactions are weak, they are effective enough to tune MoS_2 properties. Other approaches explore covalent interactions. One of them deals with the coordinative functionalisation via coordination of S atoms of MoS_2 to metal centres using metal salts.[18] Other strategies exploit the covalent functionalisation that results in the formation of S–Mo bonds at S-vacancies or C–S bonds on the basal plane.[19] While thiol derivatives are the most commonly employed molecules for the formation of S–Mo bonds,[20,21] electrophiles species, as alkyl halides and diazonium salts, have been exploited to form C–S bonds mainly due to the reactivity of the negatively charged 1T-MoS_2.[22–24] Although 2H phase has also been modified by this approach,[25,26] click chemistry has recently become an alternative to covalently functionalise this less reactive phase under mild conditions.[27]

A step further in this research area consists in introducing active molecular systems, which present bistability. Thus, smart hybrid materials can be designed to modulate the MoS_2 properties by external stimuli (light, magnetic and electric fields…).[28,29] Among active systems, photochromic bistable molecules undergo a reversible chemical conversion under light irradiation between two defined stable states, displaying markedly different physical or chemical properties. The fact that they have two defined states make them excellent candidates for developing 2D light-responsive materials, where their properties are modulated by light stimuli. Some well-known examples of photochromic molecules are azobenzenes, spiropyrans and diarylethenes.[30–32] Several researchers have focused on the use of photochromic molecules, bearing mainly azobenzene groups,[33–35] to induce optical changes into MoS_2. Nevertheless, other photochromic molecules like diarylethene derivatives remain unexplored as optical MoS_2 modulators.[36] Their photochromism arises from the reversible photoinduced cyclisation and cycloreversion reaction between the open and closed

isomers, which goes with a significant change in the electronic transport through the molecule due to the rearrangement of the π-system, with on (closed isomer) and off (open isomer) states. This effect has already been proved in molecular junctions between graphene and gold electrodes.[37–39] Therefore, diarylethene derivatives could play the role of a molecular switch in the electronic connectivity of hybrid materials when diarylethenes are used as bridges between stacked or interconnected 2D layers. Moreover, this reversible photoisomerization is accompanied by a shift of the HOMO and LUMO energy levels, which has been used to induce an optical modulation of the charge transport properties of underlying 2D materials in direct physical contact with the diarylethene molecules.[40,41] Therefore, diarylethene molecules could represent a valuable alternative as photoswitchable molecular modulators of MoS_2 flakes for optoelectronic applications. However, so far, the chemical modification of MoS_2 layers with this family of molecules remains unexplored. In this work, we demonstrate the functionalisation of chemically exfoliated MoS_2 (ce-MoS_2) flakes with a photoswitchable diarylethene molecule via electrostatic and covalent approaches (Fig. 1). In the first case, a diarylethene derivative bearing two terminal amino groups is protonated (positively charged) and mixed with negatively charged 1T ce-MoS_2 flakes. In the second case, the diarylethene derivative is used to form C–S bonds with the 2D layers by a diazotisation reaction. In both cases, the symmetrically functionalised molecules may work as molecular linkers to form stacked networks of interconnected flakes. Finally, the photoswitching capacity in solid phase of the functionalised MoS_2 materials is studied with Raman spectroscopy.

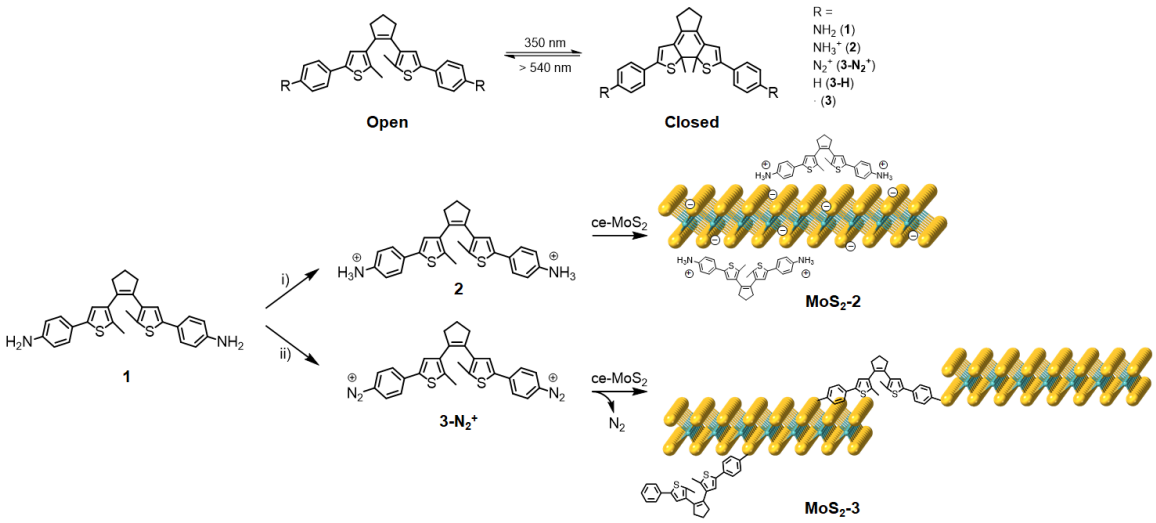

Fig. 1. Schematic representations of: (top) the photoswitching behaviour of diarylethene derivatives between the open (left) and closed isomers (right); and (bottom) the electrostatic (i: HCl in EtOH/H_2O) and covalent (ii: $NaNO_2$; HCl) functionalisation of 1T ce-MoS_2.

Results and discussion

Molecular functionalisation of ce-MoS_2

Chemically exfoliated 1T-MoS_2 was prepared by *n*-BuLi intercalation.[8] The quality of the exfoliated material and its 1T-phase nature (Fig. S1) were confirmed by X-ray powder diffraction (XRPD), X-ray photoelectron spectroscopy (XPS), ultraviolet/visible (UV/Vis) and Raman spectroscopy, transmission electron microscopy (TEM), atomic force microscopy (AFM) and thermogravimetric analysis (TGA).

Electrostatic and covalent functionalisations of ce-MoS_2 were performed using **1** in the protonated and neutral forms, respectively, with the open and closed isomers (see experimental section in the SI). **1** (and the rest of materials) denote both isomers, *i.e.* open (o) and closed (c) forms. The electrostatic approach was performed by mixing **1** at pH ~2.8 in an EtOH/H_2O solution to afford the chloride salt, **2**, and then, the addition of MoS_2, resulted in **MoS_2-2**. Impurities were removed by three washing cycles with EtOH/H_2O (2:1). The covalent functionalisation approach was carried out employing diazonium derivatives. The diazonium salts were formed in-situ by mixing **1** and sodium nitrite in a hydrochloric medium at 0 °C, under argon atmosphere.[42,43] Then, a freshly prepared aqueous suspension of ce-MoS_2 flakes was added dropwise into the reaction, and allowed to react for 24 h at room temperature. The nucleophilic attack of the negatively charged ce-MoS_2 to the electrophilic C atom of the diazonium group leads to the covalent functionalisation of the layers, **MoS_2-3**, with a new C–S bond. To remove physisorbed molecules, the product was washed with different solvents (H_2O, DMSO and MeOH) until the absence of free diarylethene molecule in solution, which

was confirmed by UV/Vis spectroscopy. For comparison purposes, physical mixture of the open isomer of the non-substituted diarylethene molecule **3-Ho** *i.e.* without anchoring groups, with ce-MoS_2 was also prepared and named as **ce-MoS_2+3-Ho**.

Characterisation

The morphology of the layers after the functionalisation processes was studied by TEM (Fig. S2), proving that the characteristic sheet-like morphology of the 2D system remains unaffected. Additionally, TEM images show the coexistence of wrinkled and non-wrinkled MoS_2 flakes. The selected-area electron diffraction (SAED) image, taken from a non-wrinkled region, presents the typical hexagonal pattern associated with MoS_2, indicating the crystalline nature of the material. The SAED image, taken from a wrinkled region, reveals diffuse rings, which would be consistent with the presence of polycrystalline material (i. e., a collection of flakes with different orientations).

Fourier-transformed infrared (FTIR) spectroscopy was used as a first approach to confirm the MoS_2 functionalisation (Fig. 2 and S3–4). Although FTIR spectra clearly prove the presence of the organic molecules on the flakes, these do not allow to discern the exclusive vibrational modes of the open and closed rings in both composites, **MoS_2-2** and **MoS_2-3**. As expected, their spectra are very similar due to the resemblance of open and closed isomers of **2** and **3-H** molecules. Interestingly, FTIR spectra of **MoS_2-2** and **MoS_2-3** present bands between 950–1640 cm^{-1}, characteristic of the C=C and C–C stretching vibrations of the photoswitchable molecule.[44] Regarding **MoS_2-3** spectra, the lack of peaks associated with aryl diazo groups[45] in the 2130 to 2315 cm^{-1} region, indicates the absence of the precursor and azocoupling adducts,[46] suggesting the covalent functionalisation to MoS_2 flakes. Although the molecule contains C–S bonds in the highly substituted thiophene rings, its characteristic stretching band is reported to appear at ~800 cm^{-1}, while the presence of a band at 664 cm^{-1}, which is absent in **MoS_2-2**, is assigned to the C–S stretching of the resultant covalent functionalisation.[26]

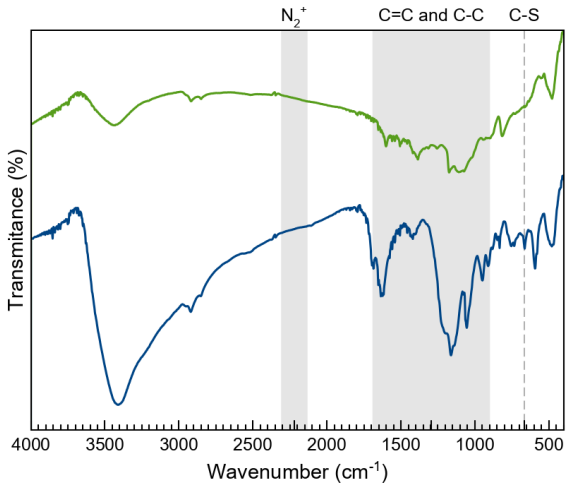

Fig. 2. FTIR spectra of **MoS_2-2o** (green) and **MoS_2-3o** (blue).

XPS spectroscopy was used to confirm the chemical composition and determine the prominent polytype in functionalised MoS_2 composites (Fig. 3). In all samples only a small amount of oxidised material is detected, showing the stability of the 2D material after functionalisation. For the sake of clarity, Table S1 summarises the Mo, S, and N XPS peaks observed in **1o, MoS_2-2**, and **MoS_2-3**.[47–51] The XPS spectra of open and closed isomers overlap perfectly in both **MoS_2-2** and **MoS_2-3**. However, clear differences can be found between the composites prepared by the electrostatic and covalent approaches. The Mo XPS spectra of **MoS_2-2** are dominated by Mo^{IV} (1T-MoS_2, 2H-MoS_2, MoO_2) peaks. In the S XPS spectra, contributions from MoS_2 and from the organic molecule can be clearly distinguished. Remarkably, the peaks associated to thiophene rings have a full width at half maximum (FWHM) of ~1.1 eV, comparable to that observed in **1o**. The region of the spectra related to N shows a clear peak at ~399.4 eV, corresponding to the amino group.[52–54] The absence of Cl in the XPS survey also supports the non-covalent functionalisation between negative-charged MoS_2 flakes and protonated amino groups. Ratios of 1T/2H MoS_2 (Mo_{1T}/Mo_{2H} = ~0.33 and 0.48 for open and closed forms, respectively) were calculated from Mo normalised areas, reflecting the coexistence of these phases in both hybrid materials in spite of an increase of the 2H phase, when compared with freshly prepared ce-MoS_2.

The XPS Mo spectra of **MoS_2-3** are dominated by Mo^{IV} (2H-MoS_2, MoO_2) peaks. Apart from that, it is important to remark that for the S spectra, the peaks ascribed to S–C bonds are broader (with a FWHM of ~1.5 eV) than those assigned to aromatic S–C from the thiophene in **1o** (with a FWHM of ~1.1 eV). This fact confirms that new covalent bonds, as well as the thiophene rings, contribute to S–C peaks. Consistently, **MoS_2-3** does not reveal clear N signals in the N 1s region, suggesting that no nitrogen-containing by-products (like azo derivatives), or starting materials are present. Therefore, the absence of N peaks and the detection of broader S–C signals prove the efficacy of diazo moieties as leaving groups and the attachment of the diarylethene backbone to ce-MoS_2 flakes. Furthermore, Mo XPS spectra suggest that the 1T-MoS_2, obtained by the chemical exfoliation with *n*-BuLi, have been completely transformed into the most thermodynamically stable 2H-MoS_2.

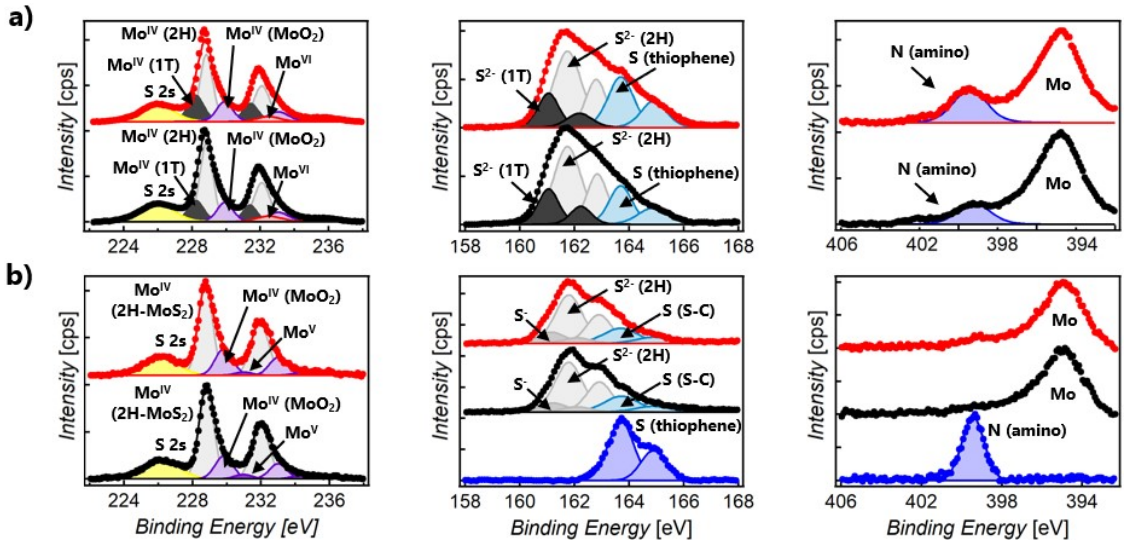

Fig. 3. Normalised Mo 3d (left), S 2p (middle) and N 1s spectra (right) of electrostatic (a) and covalent functionalised compounds (b). Each XPS spectrum is normalised respect to the highest value registered in its envelope. Colour code: a, **MoS_2-2o** (black) and **MoS_2-2c** (red); b, **MoS_2-3o** (black), **MoS_2-3c** (red) and **1o** (blue).

The XRPD patterns of **MoS_2-2** and **MoS_2-3** resemble that of restacked ce-MoS_2 (Fig. 4). The most intense peak at ~14.3° (6.2 Å) corresponds to the (002) plane of bulk MoS_2, which indicates that some non-exfoliated MoS_2 stacks are still present after the exfoliation. However, the broadening of (002) peaks in comparison to that peak observed in the diffraction pattern of bulk MoS_2, is consistent with a drop in the periodicity along the *c*-axis, which is due to the decrease in the number of stacked layers (few-layers MoS_2). Moreover, defects from the exfoliation and functionalization treatments can also contribute to this broadening.[55–57] The detection of (00*l*) peaks below 2θ ~14.3° shows that there are restacked layers with larger interlayer distances than in the bulk. In ce-MoS_2, this peak appears at 2θ ~7.2°, and is commonly related to water bilayers between MoS_2 monolayers.[58,59] In the electrostatic composite, **MoS_2-2c**, such peak is slightly shifted to ~6.4°, corresponding to a interlayer spacing of 13.8 Å. This observation could be indicative of the presence of **2c** molecules forming a monolayer or bilayer, depending on the orientation adopted by the flexible molecule on the MoS_2 layer (Fig. S5).

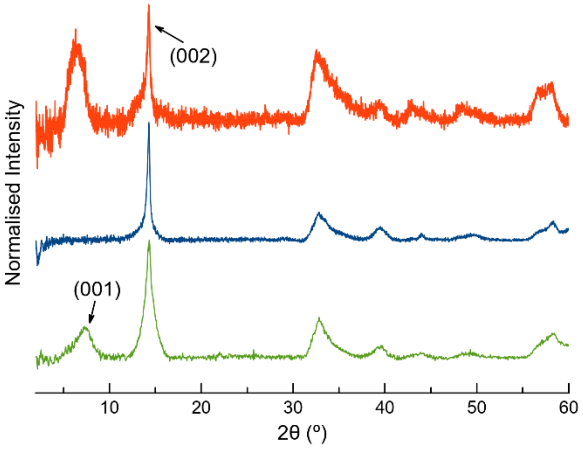

Fig. 4. Normalised XRPD patterns of restacked ce-MoS_2 flakes (green), **MoS_2-3c** (blue) and **MoS_2-2c** (orange).

In contrast, no peaks below ~14.3° are observed in the covalent composite **MoS_2-3**. The presence of peaks at low 2θ values is usually ascribed to the presence of the molecule and suggests a covalent functionalisation of the basal plane. Still, its absence in **MoS_2-3** might be related to the loss of large periodicity in the *c*-axis. Unlike Rao *et al.* who claimed layered assemblies by using a rigid linker,[23] the photochromic diarylethene molecules can either connect to different MoS_2 layers or react with just one of them due to their flexibility. Then, such pillared structures might not be formed along the whole *c*-axis, or they can present inhomogeneous interlayer distances (no periodicity). Furthermore, the absence of the peak at 2θ ~7.2°, related to a bilayer of water molecules between the MoS_2 layers, can also be justified by the use of more volatile solvents during the last purification step, in the synthesis of the composite.

Raman spectroscopy was performed in a second step to distinguish between the open- and closed-ring isomers of the photochromic molecule. Three different excitation wavelengths (532, 633, and 785 nm) were tested in order to find the optimum conditions.

The Raman spectra of **2** as solid are mainly masked due to the presence of a strong photoluminescence (PL), with low resolved peaks associated to the closed-ring isomer, while no peaks are detected for the open one (Fig. S6). In **MoS_2-2**, the attachment of **2** on MoS_2 leads to the PL quenching of the organic system, probably caused by a charge transfer between the layer and the organic molecule (Fig. 5). Regarding MoS_2, the characteristic peaks of the 1T phase are clearly visible at ~152 (J_1) and 328 cm^{-1} (J_3). The most intense peaks detected in **MoS_2-2** spectra somehow match with those registered for **2c**, which intriguingly suggests the presence of the closed-ring isomer in both **MoS_2-2** composites. It has been previously reported that a reductive cyclisation of the open isomer can be induced in some diarylethene derivatives.[60] Moreover, ce-MoS_2 can act as a reducing agent due to the accumulation of negative charge after its chemical exfoliation.[8] Thus, in this scenario, a reduction/cyclisation of **2o** becomes possible when the molecule contacts with the 2D layer, which is reflected in the Raman spectra and in the increased percentage of 2H-MoS_2 phase.

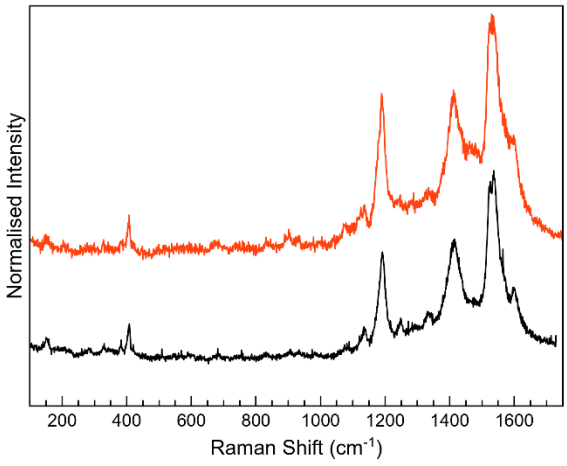

Fig. 5. Normalised Raman at 532 nm excitation wavelength for **MoS_2-2o** (black) and **MoS_2-2c** (red).

For **3-H**, the best Raman resolution was obtained at an exciton wavelength of 785 nm (Fig. S7). Although **3-H** exhibits PL when more energetic lasers are used (Fig. S7), **3-H** and MoS_2 features are perfectly visible in the **MoS_2-3** composite at 532 nm (Fig. 6a), indicating, again, a PL quenching and therefore a potential charge transfer between the organic and the inorganic components. While the peaks at ~382 and 407 cm^{-1} correspond to E^1_{2g} and A_{1g} vibrational modes of MoS_2, the peaks located in the 1100–1700 cm^{-1} range are assigned to the organic molecule,[44] which are slightly blue-shifted with respect to those arising from **MoS_2-2**. Remarkably, peaks assigned to the organic molecule in the composite are very different from those in pure **3-H** molecules (Fig. S7). These changes can be caused by the formation of new C–S bonds due to the high electronic sensitivity of the molecule towards aromatic rings substitution[44] and additionally, to the constraints imposed by the 2D material.

The Raman peaks assigned to the organic molecule are ~1141, 1196, 1403, 1439, 1520 and 1597 cm^{-1} for **MoS_2-3o** and 1191, 1521 and 1593 cm^{-1} for **MoS_2-3c**. However, weak peaks at ~1141 and 1403 cm^{-1} attributed to **MoS_2-3o** are also visible in **MoS_2-3c.** This fact is ascribed to the synthetic procedure of the closed form of the molecule (see SI), where the cyclisation reaction is stopped before reaching the entire conversion. Hence, some **MoS_2-3o** might be present as a small impurity. No *J* peaks (characteristic of 1T-MoS_2) were detected in **MoS_2-3** spectra,[61] confirming the 2H-MoS_2 nature already determined by XPS. This fact was also supported by the presence of PL with two bands related to the A_1 and B_1 excitonic transitions at ~1.77 and 1.95 eV, characteristic of the 2H phase (Fig. 6b).

MoS_2-2, **MoS_2-3** and the organic molecule **3-Ho** were characterised by TGA analysis (Fig. S8). Whereas the electrostatic composite **MoS_2-2** presents a larger mass loss for the open than for the closed-ring isomer, similar TGA curves were recorded for both isomers of the covalent composite, **MoS_2-3**. For all four samples, an initial weight loss lower than 5%, occurs between 25 °C and 140 °C corresponding to the release of physisorbed solvent molecules. Then, in the case of **MoS_2-2**, a significantly different weight loss of ~23.1 and ~12.5% in the 140–700 °C range were found for the open and closed composites. In **MoS_2-3**, a mass drop of ~27.4% and ~21.9% in two continuous steps was detected in the 140–700 °C range for the open and closed composites, respectively. The mass loss in the 140–700 °C range arises from the removal of the organic molecules attached to the MoS_2, except for a small contribution (~3.1%) corresponding to the S degradation of MoS_2 in all samples. With those considerations, the ratios molecule:MoS_2 for **MoS_2-2o** and **MoS_2-2c** were estimated as 0.09 and 0.04 while for **MoS_2-3** values of 0.13 and 0.09 were estimated for the open and closed isomers, respectively. These ratios should be slightly larger due to the small amount of oxidised Mo observed by XPS that has not been considered.

In order to get further information, a mechanical mixture of ce-MoS_2 and **3-Ho** (**ce-MoS_2+3-Ho**) was prepared and measured by TGA in the same conditions. As can be seen in Fig. S8, the loss of the organic molecule in the mechanical mixture is sharp and takes place at almost the same temperature than the free organic molecule. However, in **MoS_2-2** or **MoS_2-3** composites, the loss of the organic component is much more gradual and shifted to higher temperatures. These observations highlight the effective interaction between MoS_2 layers and the diarylethene molecules, supporting an effective functionalisation of the layers, although a difference in the strength between electrostatic and covalent interactions is not evident. Moreover, we note that the functionalisation degree of the electrostatic composite is smaller. This could be related to an efficient removal of molecules during the washing steps in the synthetic protocol. In contrast, this removal is not possible in the covalent composite since the molecules are strongly bonded. Additionally, the difference between the open and closed isomers of the electrostatic composite could point out to the difficulty of the less flexible closed molecule to accommodate on the MoS_2 surface (Fig. S5).

Photoswitching behaviour study of composites.

Photoswitchable studies were performed on both isomers of **MoS_2-2** and **MoS_2-3**. To gain more insight into the photoswitchable behaviour, these studies were also performed on the organic molecules, **2** and **3-H**. As observed in other protonated diarylethene derivatives,[62] **2** presents a unidirectional switching from open to closed isomers upon UV light irradiation, $\lambda = 350$ nm, that cannot be reverted upon illumination with visible light, λ = 533 nm (Fig. S9). Regarding **3-H**, photoactive open and closed isomers are confirmed by reversible UV/Vis spectra evolution (Fig. S10).

Although UV/Vis spectroscopy is a useful technique for colour changes, this is not the case here, since the strong absorption of MoS_2 masks the absorption bands from organic molecules in these materials (Fig. S11), thus, preventing to clearly distinguish between closed and open forms. While the organic molecules are soluble systems, the prepared composites are unstable suspensions that precipitate during long term experiments. In order to perform all experiments in equivalent conditions, the selected material was deposited onto clean SiO_2 (285nm)/Si substrates by drop-casting of their suspensions/solutions. Samples **2** and **3-H** were irradiated with a photoreactor at 350 nm and >540 nm at different times and were studied by

Raman spectroscopy (Figs. S12 and 13). Open- to closed-ring isomer transformation was observed for **2** and **3-H** at 350 nm irradiation wavelength, while the reverse ring-opening only occurs for **3-H** at >540 nm as expected by the photoswitching behaviour observed in the absorption spectra.

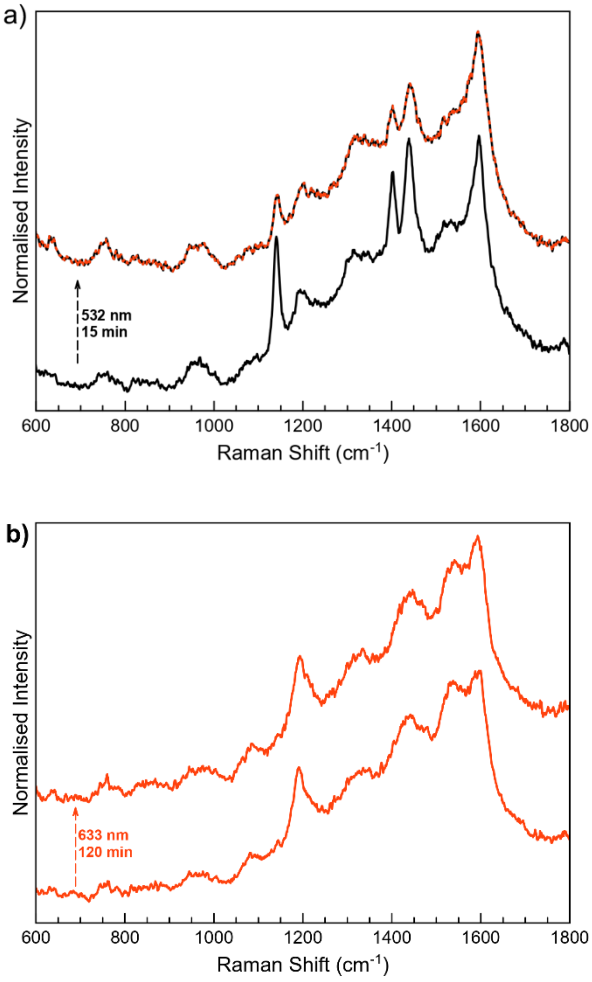

Fig. 7. Raman spectra for the irradiated **MoS_2-3o** (a) and **MoS_2-3c** (b) samples deposited on SiO_2 measured with a 532 nm excitation laser with 1% laser power. The open-ring isomer, the closed-ring isomer and a mixture of open-ring and closed-ring isomers are represented as black, red and black-red lines, respectively. The spectra were normalised for comparison purposes.

Regarding **MoS_2-2** and **MoS_2-3** composites, first attempts inside the photoreactor at the same irradiation wavelengths as the organic molecules did not affect their Raman spectra (Figs. S14 and S15). Thus, as an alternative approach, composite samples were irradiated at different wavelengths and measured in-situ on the same spot area with the Raman spectrophotometer at 532 nm (see SI for experimental details).
Then, Raman irradiation experiments of **MoS_2-2** at all available wavelengths revealed again that both isomers behaved identically under light irradiation, i. e., no significant changes in the spectra were detected, only a signal attenuation (Fig. S16). This fact is not surprising since, as previously described, Raman spectra of **MoS_2-2c** and **MoS_2-2o** are the same, pointing out the possibility of the presence of **2c** in both (Fig. 5). Thus, **MoS_2-2c** is a photoinactive composite as the diarylethene derivative **2c** is.
MoS_2-3 was locally irradiated and measured in-situ with a Raman spectrometer (Fig. 7). Irradiation of **MoS_2-3o** was performed at the lowest wavelengths available in the spectrometer. First experiments at 473 nm did

not induce any change in the Raman spectra; however, after irradiation at 532 nm during 15 minutes, the intensity of the peaks at ~1140, 1403 and 1439 cm^{-1} decreases. These results are indicative of a successful (although incomplete) open-closed photoconversion. Attempts to revert this change by irradiation at larger wavelengths (633 nm) seem to revert Raman peaks to the open form. However, this result was sample dependent, with low reproducibility, so it cannot be considered conclusive (Fig. S17). Unidirectional switching has also been previously observed in diarylethene derivatives attached to different surfaces, and it has been blamed on the strong coupling through the covalent bonds.[37,38,63,64]

Remarkably, the observed excitation wavelengths are significantly shifted from those responsible for the photoswitching processes in the free molecule **3-H**. This difference can be due to the strong modification of the electronic structure of **3-H** once covalent C–S bonds between the diarylethene unit and the extended MoS_2 network are formed. This fact can significantly perturb the orbitals responsible for the cyclisation and cycloreversion steps, and therefore, the absorption spectrum.[65] Higher wavelengths than the ones used for the photoswitching of free diarylethene molecules have also been observed when diarylthene molecules work as coordination ligands in iridium complexes.[66,67]

Next, when **MoS_2-3c** was irradiated at 532 nm and 633 nm (Fig. 7b), no changes were observed at the 600–1800 cm^{-1} region, even increasing the laser power or the irradiation time. The differences in the photoswitching behaviour of the directly synthetised open and closed composites **MoS_2-3** could be influenced by the different way that open and closed diarylethene molecules can be anchored to the surface (due to different geometry and mobility) and, consequently, by a different limitation of the molecular movement in the resulting composite. By means of a molecular editor and visualizer software (Avogadro), we have studied in more detail the structure of the diarylethene derivatives used in this work. Geometrical restrictions could be significant when a diarylethene molecule is covalently bonded to the same MoS_2 flake through the two phenyls groups (low probability due to the molecular structure of the molecule). However, these restrictions are reduced if the molecule connects two different flakes or is asymmetrically anchored by only one phenyl group. Due to the structural differences between open and closed isomers (Fig. S5), a double anchoring to the same MoS_2 flake is even less probable for the open form, and therefore fewer mobility restrictions are expected for this isomer in the final composite. Remarkably, a diastereoselective cyclisation on hydrogen-bond confined diarylethene switches has already been observed, emphasising the importance of geometrical restrictions.[68]

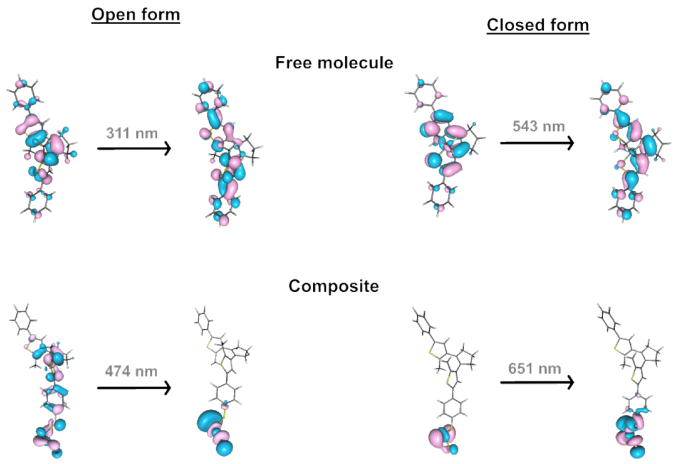

Fig. 8 Perspective views of the natural transition orbitals (NTOs) involved in some significant theoretical electronic excitations of the open and closed forms of the organic molecule and composite. The isodensity surfaces correspond to a cut-off value of 0.05 e $bohr^{-3}$. Electrons are promoted from the orbital at the left side to the other one at the right side.

To cast light on the experimental observations, the nature of some electronic excitations involved in the photochemical processes of **MoS_2-3** composites was theoretically studied. Models used for this purpose are detailed in the Supporting Information (Section 9 and Fig. S18).

In the free organic molecule, the closure and aperture of the cycle occur at 310 and 540 nm. For an electronic excitation, donor and acceptor anti-bonding and bonding molecular orbitals, respectively, make the formation of the cycle possible, and conversely, they cause its opening (Fig. 8 and Fig. S19). When dealing with the formation of composites, the anchoring of the organic molecule to a MoS_2 layer involves creating a radical lying on the carbon atom of the molecule directly linked to the sulphur atom of the 2D layer. However,

the spin density on this atom is delocalised on the layer, which transfers one electron to the attached molecule (Fig. S20). This situation changes the electronic and photochemical properties of the lying molecules. Thus, several lower excited states appear, which are reached through electronic excitations whose ligand-metal charge transfer (LMCT) nature weakens the previously mentioned bonding-antibonding counterbalance responsible for the cyclization and its opening (Fig. S21). The presence of such states provides a path for relaxation to the starting state, inhibiting the cyclization process and the reverse, explaining why more energetic light sources, such as those that work on free molecules (350 and 540 nm), do not work in **MoS_2-3**. Therefore, the presence of these excited states, together with the fact that the oscillator strengths and the intensity of the absorptions are lower in **MoS_2-3**, suggest that the photoswitching process must be less efficient, as experimentally observed. Moreover, despite the main contribution of the layer in the acceptor orbital in an electronic excitation in **MoS_2-3**, the decrease of the antibonding nature between carbon atoms for the electronic excitation at 474 nm (carbon atoms which are not bonded in the donor orbital), would partially favour cyclization, which may explain the experimental results observed under irradiation at 535 nm (Fig. S21).

Hence, future work should be performed to avoid the hindering of the photoswitching process, probably influenced by diarylethene mobility restrictions, but mainly affected by the strong coupling with the MoS_2 layer once anchored to the surface. In this scenario, one potential strategy could deal with the use of symmetric or asymmetric diarylethene molecules including longer substituents which would permit more flexibility and the electronic isolation of the diarylethene core from the surface.

Conclusions

This work shows for the first time, MoS_2 functionalised with photoswitchable diarylethene molecules by electrostatic and covalent forces. Electrostatic functionalisation is performed by exploiting the charge interactions between the positive-charged photochromic molecule and the negative-charged ce-MoS_2 flakes. Furthermore, the covalent functionalisation of ce-MoS_2 flakes is achieved by the well-known diazonium salt strategy.

By the electrostatic approach, the final composites obtained by using both, the open or the closed-ring diarylethene isomers, present identical Raman spectra and irreversible photoswitchable behaviour. Moreover, there is a charge transfer interaction between the deposited molecules and the layers, which is demonstrated by the quenching of the PL of the diarylethene derivative. Interestingly, experimental results point out a partial cyclisation of the open-ring molecule when it gets in contact with the ce-MoS_2 layers, probably due to the reducing role of the 2D layer. Consequently, ce-MoS_2 layers undergo a partial phase transition, which is unexpected for pure electrostatic interactions between the molecule and the 2D material.

Following the covalent strategy, the symmetric diarylethene molecules present two equivalent anchoring groups that can induce a cross-linking effect. However, the lack of a new periodicity observed in the *c*-axis is indicative of limited cross-linking and inhomogeneous interlayer distances. Through the covalent approach, the open and the closed-ring diarylethene isomers give rise to composites with a different Raman footprint, reflecting the stability of both isomers in contact with the MoS_2 layers. As proven by Raman spectroscopy and XPS, during the functionalisation process, 1T-MoS_2 is totally transformed into the 2H polytype, which can be due to a decrease of the negative charge accumulated on the layer when new covalent bonds are formed. Like in the electrostatic composite, the quenching of diarylethene PL denotes a charge transfer interaction between organic and inorganic components.

Irradiations experiments reveal that the open form for the covalently functionalised MoS_2 undergoes partial close-open reactions. However, going from closed to open material is not possible under the established experimental conditions. Theoretical calculations support that the main reason behind this ineffective switching is the modification of the excited states involved in the process and the emergence of other less energetic states, which is originated by the anchoring of the molecule on the MoS_2 sheet and the emergence of a radical character in the composite.

The study of these molecular/2D heterostructures may be of interest to tune the MoS_2 properties via the interactions established with the molecular component. Diarylethenes are envisioned as components of electronic devices due to their switchable properties induced by light, which in the present case, can be attached to 2D materials to afford 2D-light-responsive hybrid systems. The photoswitching effect on the MoS_2 layer for the reported composites will be further studied in the near future.

Conflicts of interest

There are no conflicts to declare.

Acknowledgements

The authors acknowledge the financial support from the EU (ERC-Advanced Grant MOL-2D 788222 and FET-OPEN COSMICS 766726), the Spanish MICINN (Grants MAT2017-89993, Excellence Unit María de Maeztu CEX2019-000919-M, PID2019-109735GB-100, PID2019-104778GB-100 and EQC2018-004888-P, EQC2019-005816-P cofinanced by FEDER), and the Generalitat Valenciana (Prometeo Program of Excellence, PO FEDER Program IDIFEDER/2018/061, IDIFEDER/2020/063). M.M.-G. thanks the Spanish MECD for the award of a FPU Grant. J.M.C.-V. thanks the Spanish MICINN for his F.P.I Grant.

References

1 S. Z. Butler, S. M. Hollen, L. Cao, Y. Cui, J. A. Gupta, H. R. Gutiérrez, T. F. Heinz, S. S. Hong, J. Huang, A. F. Ismach, E. Johnston-Halperin, M. Kuno, V. V. Plashnitsa, R. D. Robinson, R. S. Ruoff, S. Salahuddin, J. Shan, L. Shi, M. G. Spencer, M. Terrones, W. Windl and J. E. Goldberger, *ACS Nano*, 2013, **7**, 2898–2926.

2 C. N. R. Rao, A. K. Sood, K. S. Subrahmanyam and A. Govindaraj, *Angew. Chemie Int. Ed.*, 2009, **48**, 7752–7777.

3 D. Lembke and A. Kis, *ACS Nano*, 2012, **6**, 10070–10075.

4 G. Eda and S. A. Maier, *ACS Nano*, 2013, **7**, 5660–5665.

5 H. Wang, C. Li, P. Fang, Z. Zhang and J. Z. Zhang, *Chem. Soc. Rev.*, 2018, **47**, 6101–6127.

6 M. Donarelli and L. Ottaviano, *Sensors*, 2018, **18**, 3638.

7 H. S. Nalwa, *RSC Adv.*, 2020, **10**, 30529–30602.

8 M. Morant-Giner, R. Sanchis-Gual, J. Romero, A. Alberola, L. García-Cruz, S. Agouram, M. Galbiati, N. M. Padial, J. C. Waerenborgh, C. Martí-Gastaldo, S. Tatay, A. Forment-Aliaga and E. Coronado, *Adv. Funct. Mater.*, 2018, **28**, 1706125.

9 Y. Wang, J. Mao, X. Meng, L. Yu, D. Deng and X. Bao, *Chem. Rev.*, 2019, **119**, 1806–1854.

10 R. J. Toh, Z. Sofer, J. Luxa, D. Sedmidubský and M. Pumera, *Chem. Commun.*, 2017, **53**, 3054–3057.

11 W. Zhao, J. Pan, Y. Fang, X. Che, D. Wang, K. Bu and F. Huang, *Chem. - A Eur. J.*, 2018, **24**, 15942–15954.

12 A. Stergiou and N. Tagmatarchis, *Chem. – A Eur. J.*, 2018, **24**, 18246–18257.

13 S. Bertolazzi, M. Gobbi, Y. Zhao, C. Backes and P. Samorì, *Chem. Soc. Rev.*, 2018, **47**, 6845–6888.

14 J. Kibsgaard, Z. Chen, B. N. Reinecke and T. F. Jaramillo, *Nat. Mater.*, 2012, **11**, 963–969.

15 H. Nan, Z. Wang, W. Wang, Z. Liang, Y. Lu, Q. Chen, D. He, P. Tan, F. Miao, X. Wang, J. Wang and Z. Ni, *ACS Nano*, 2014, **8**, 5738–5745.

16 L. Daukiya, J. Seibel and S. De Feyter, *Adv. Phys. X*, 2019, **4**, 1625723.

17 D. Iglesias, S. Ippolito, A. Ciesielski and P. Samorì, *Chem. Commun.*, 2020, **56**, 6878–6881.

18 S. Lei, X. Wang, B. Li, J. Kang, Y. He, A. George, L. Ge, Y. Gong, P. Dong, Z. Jin, G. Brunetto, W. Chen, Z.-T. Lin, R. Baines, D. S. Galvão, J. Lou, E. Barrera, K. Banerjee, R. Vajtai and P. Ajayan, *Nat. Nanotechnol.*, 2016, **11**, 465–471.

19 P. Vishnoi, A. Sampath, U. V. Waghmare and C. N. R. Rao, *Chem. - A Eur. J.*, 2017, **23**, 886–895.

20 D. M. Sim, M. Kim, S. Yim, M.-J. Choi, J. Choi, S. Yoo and Y. S. Jung, *ACS Nano*, 2015, **9**, 12115–12123.

21 M. Makarova, Y. Okawa and M. Aono, *J. Phys. Chem. C*, 2012, **116**, 22411–22416.

22 H. Lee, S. Bak, S.-J. An, J. H. Kim, E. Yun, M. Kim, S. Seo, M. S. Jeong and H. Lee, *ACS Nano*, 2017, **11**, 12832–12839.

23 K. Pramoda, U. Gupta, I. Ahmad, R. Kumar and C. N. R. Rao, *J. Mater. Chem. A*, 2016, **4**, 8989–8994.

24 K. C. Knirsch, N. C. Berner, H. C. Nerl, C. S. Cucinotta, Z. Gholamvand, N. McEvoy, Z. Wang, I. Abramovic, P. Vecera, M. Halik, S. Sanvito, G. S. Duesberg, V. Nicolosi, F. Hauke, A. Hirsch, J. N. Coleman and C. Backes, *ACS Nano*, 2015, **9**, 6018–6030.

25 Y. Park, S. Shin, Y. An, J.-G. Ahn, G. Shin, C. Ahn, J. Bang, J. Baik, Y. Kim, J. Jung and H. Lim, *ACS Appl. Mater. Interfaces*, 2020, **12**, 40870–40878.

26 X. S. Chu, A. Yousaf, D. O. Li, A. A. Tang, A. Debnath, D. Ma, A. A. Green, E. J. G. Santos and Q. H. Wang, *Chem. Mater.*, 2018, **30**, 2112–2128.

27 M. Vera-Hidalgo, E. Giovanelli, C. Navío and E. M. Pérez, *J. Am. Chem. Soc.*, 2019, **141**, 3767–3771.

28 R. Torres-Cavanillas, M. Morant-Giner, G. Escorcia-Ariza, J. Dugay, S. Tatay, S. Cardona-Serra, M. Giménez Marqués, M. Galbiati, A. Forment-Aliaga and E. Coronado, *ChemRxiv* , 2020, https://doi.org/10.26434/chemrxiv.12664799.v1

29 Y. Zhao, S. Bertolazzi, M. S. Maglione, C. Rovira, M. Mas-Torrent and P. Samorì, *Adv. Mater.*, 2020, **32**, 2000740.
30 B. L. Feringa and W. R. Browne, Eds., *Molecular Switches*, Wiley-VCH Verlag GmbH & Co. KGaA, Weinheim, Germany, 2011.
31 M. Irie, *Chem. Rev.*, 2000, **100**, 1685–1716.
32 M. Irie, T. Fukaminato, K. Matsuda and S. Kobatake, *Chem. Rev.*, 2014, **114**, 12174–12277.
33 J. Li, J. Wierzbowski, Ö. Ceylan, J. Klein, F. Nisic, T. Le Anh, F. Meggendorfer, C.-A. Palma, C. Dragonetti, J. V. Barth, J. J. Finley and E. Margapoti, *Appl. Phys. Lett.*, 2014, **105**, 241116.
34 L. Cabral, F. P. Sabino, M. P. Lima, G. E. Marques, V. Lopez-Richard and J. L. F. Da Silva, *J. Phys. Chem. C*, 2018, **122**, 18895–18901.
35 Y. Zhao, S. Bertolazzi and P. Samorì, *ACS Nano*, 2019, **13**, 4814–4825.
36 S.-Z. Pu, Q. Sun, C.-B. Fan, R.-J. Wang and G. Liu, *J. Mater. Chem. C*, 2016, **4**, 3075–3093.
37 D. Dulić, S. J. van der Molen, T. Kudernac, H. T. Jonkman, J. J. D. de Jong, T. N. Bowden, J. van Esch, B. L. Feringa and B. J. van Wees, *Phys. Rev. Lett.*, 2003, **91**, 207402.
38 C. Jia, A. Migliore, N. Xin, S. Huang, J. Wang, Q. Yang, S. Wang, H. Chen, D. Wang, B. Feng, Z. Liu, G. Zhang, D.-H. Qu, H. Tian, M. A. Ratner, H. Q. Xu, A. Nitzan and X. Guo, *Science (80-.).*, 2016, **352**, 1443–1445.
39 D. Kim, H. Jeong, W.-T. Hwang, Y. Jang, D. Sysoiev, E. Scheer, T. Huhn, M. Min, H. Lee and T. Lee, *Adv. Funct. Mater.*, 2015, **25**, 5918–5923.
40 H. Qiu, Z. Liu, Y. Yao, M. Herder, S. Hecht and P. Samorì, *Adv. Mater.*, 2020, **32**, 1907903.
41 H. Qiu, Y. Zhao, Z. Liu, M. Herder, S. Hecht and P. Samorì, *Adv. Mater.*, 2019, **31**, 1–7.
42 S. Baranton and D. Belanger, *J. Phys. Chem. B*, 2005, **109**, 24401–24410.
43 D. Hetemi, V. Noël and J. Pinson, *Biosensors*, 2020, **10**, 4.
44 J. J. D. de Jong, W. R. Browne, M. Walko, L. N. Lucas, L. J. Barrett, J. J. McGarvey, J. H. van Esch and B. L. Feringa, *Org. Biomol. Chem.*, 2006, **4**, 2387–2392.
45 K. Nakamoto, *Infrared and Raman Spectra of Inorganic and Coordination Compounds*, John Wiley & Sons Inc., New York, 4th edn., 1997.
46 S. Mahouche-Chergui, S. Gam-Derouich, C. Mangeney and M. M. Chehimi, *Chem. Soc. Rev.*, 2011, **40**, 4143–4166.
47 O. L. Li, Z. Shi, H. Lee and T. Ishizaki, *Sci. Rep.*, 2019, **9**, 12704.
48 J. Baltrusaitis, P. M. Jayaweera and V. H. Grassian, *Phys. Chem. Chem. Phys.*, 2009, **11**, 8295.
49 Y. Sun, X. Hu, W. Luo and Y. Huang, *J. Mater. Chem.*, 2012, **22**, 425–431.
50 J.-G. Choi and L. T. Thompson, *Appl. Surf. Sci.*, 1996, **93**, 143–149.
51 X. Geng, W. Sun, W. Wu, B. Chen, A. Al-Hilo, M. Benamara, H. Zhu, F. Watanabe, J. Cui and T. Chen, *Nat. Commun.*, 2016, **7**, 10672.
52 Q. Liu, X. Li, Q. He, A. Khalil, D. Liu, T. Xiang, X. Wu and L. Song, *Small*, 2015, **11**, 5556–5564.
53 F. Z. Wang, M. J. Zheng, B. Zhang, C. Q. Zhu, Q. Li, L. Ma and W. Z. Shen, *Sci. Rep.*, 2016, **6**, 31092.
54 M. Kehrer, J. Duchoslav, A. Hinterreiter, M. Cobet, A. Mehic, T. Stehrer and D. Stifter, *Plasma Process. Polym.*, 2019, **16**, 1800160.
55 H. Jensen, J. H. Pedersen, J. E. JØrgensen, J. S. Pedersen, K. D. Joensen, S. B. Iversen and E. G. SØgaard, *J. Exp. Nanosci.*, 2006, **1**, 355–373.
56 G. Du, Z. Guo, S. Wang, R. Zeng, Z. Chen and H. Liu, *Chem. Commun.*, 2010, **46**, 1106–1108.
57 T. Ungár, *Scr. Mater.*, 2004, **51**, 777–781.
58 T. Mahmood, M. Arshad, M. A. Gilani, Z. Iqbal and K. Ayub, *J. Mol. Model.*, 2015, **21**, 321.
59 M. Acerce, D. Voiry and M. Chhowalla, *Nat. Nanotechnol.*, 2015, **10**, 313–318.
60 B. Gorodetsky, H. D. Samachetty, R. L. Donkers, M. S. Workentin and N. R. Branda, *Angew. Chemie Int. Ed.*, 2004, **43**, 2812–2815.
61 N. H. Attanayake, A. C. Thenuwara, A. Patra, Y. V. Aulin, T. M. Tran, H. Chakraborty, E. Borguet, M. L. Klein, J. P. Perdew and D. R. Strongin, *ACS Energy Lett.*, 2018, **3**, 7–13.
62 H. Liu, X. Zhang, Z. Gao and Y. Chen, *J. Phys. Chem. A*, 2012, **116**, 9900–9903.
63 A. C. Whalley, M. L. Steigerwald, X. Guo and C. Nuckolls, *J. Am. Chem. Soc.*, 2007, **129**, 12590–12591.
64 C. Jia, J. Wang, C. Yao, Y. Cao, Y. Zhong, Z. Liu, Z. Liu and X. Guo, *Angew. Chemie Int. Ed.*, 2013, **52**, 8666–8670.
65 A. Staykov, J. Areephong, W. R. Browne, B. L. Feringa and K. Yoshizawa, *ACS Nano*, 2011, **5**, 1165–1178.
66 W. Tan, Q. Zhang, J. Zhang and H. Tian, *Org. Lett.*, 2009, **11**, 161–164.
67 W. Tan, J. Zhou, F. Li, T. Yi and H. Tian, *Chem. – An Asian J.*, 2011, **6**, 1263–1268.
68 K. Uchida, M. Walko, J. J. D. de Jong, S. Sukata, S. Kobatake, A. Meetsma, J. van Esch and B. L. Feringa, *Org. Biomol. Chem.*, 2006, **4**, 1002.

Supporting Information

Functionalisation of MoS_2 2D layers with diarylethene molecules

†Marc Morant-Giner,[a] †José Miguel Carbonell-Vilar,[a] Marta Viciano-Chumillas,[a,*] Alicia Forment-Aliaga,[a,*] Joan Cano,[a] Eugenio Coronado[a]

1 Experimental

Materials

All chemicals were obtained from commercial sources and used as received. 1,2-bis(5-chloro-2-methylthien-3-yl)cyclopentene (**a**) and 1,2-bis(2-methyl-5-phenylthien-3-yl)cyclopentene (**3-H**) were synthesised following the reported procedures.[1] ce-MoS_2 was synthesised by solvothermal lithium intercalation according to the reported procedure.[2]

Caution! Diazonium salts are potentially explosive. They should be used in small quantities and be treated with the utmost care at all times.

1.1 Syntheses of the organic molecules

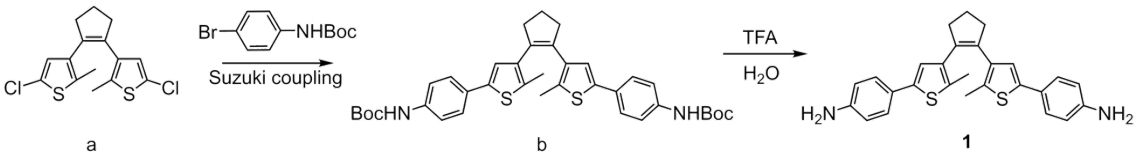

Scheme 1. Synthetic procedure of **1**.

1,2-Bis[2-methyl-5-(4-*N*-(*tert*-butoxycarbonyl)-aminophenyl)-3-thienyl]cyclopentene (b). **a** (0.58 g, 1.76 mmol) and 13 mL of dry THF were added into a two-necked flask under an argon atmosphere. Then, *n*-butyllithium (2.30 mL, 3.69 mmol, 1.6 M in hexane) was very slowly added, giving a black solution. Next, tributyl borate (1.42 mL, 5.26 mmol) was quickly added affording an orange solution, which was stirred for 1 h at room temperature. Then, *N*-(*tert*-butoxycarbonyl)-4-bromoaniline (1.43 mg, 5.27 mmol), $Pd(PPh_3)_4$ (203 mg, 0.18 mmol), sodium carbonate (11.40 mL, 22.83 mmol, 2 M in H_2O) and few drops of ethylene glycol were added sequentially to the reaction mixture, which was refluxed overnight. The reaction cooled down to room temperature and, then, H_2O (120 mL) was added. Liquid-liquid extraction was performed by adding ethyl acetate (2 × 55 mL). The organic phase was washed with brine, dried over magnesium sulphate, and the solvent was removed in a rotary evaporator giving a reddish-brown oil. The product was purified by column chromatography on silica gel (8.5 hexane: 1.5 ethyl acetate) affording a brown solid (0.64 g, 60%). ^{1}H-NMR (300 MHz, $CDCl_3$) δ = 7.43 (d, *J* = 8.62 Hz, 4H, phenyl), 7.34 (d, *J* = 8.80 Hz, 4H, phenyl), 6.97 (s, 2H, thiophene), 6.60 (s, 2H, NH), 2.85 (t, *J* = 7.52 Hz, 4H, cyclopentene), 2.08 (qt, *J* = 7.52 Hz, 2H, cyclopentene), 1.99 (s, 6H, CH_3), 1.54 (s, 18H, CH_3).

1,2-Bis[2-methyl-5-(4-aminophenyl)-3-thienyl]cyclopentene (1o). **b** (0.64 g, 1 mmol) was dissolved in dichloromethane (25 mL). Next, trifluoroacetic acid (2.48 mL, 53.08 mmol) was added and stirred vigorously overnight and, later, the solvent was removed in a rotary evaporator. Saturated sodium bicarbonate (35 mL) was added and extracted with dichloromethane (6 × 20 mL). The organic phase was collected, dried over magnesium sulphate and filtered under vacuum, giving a red solution. The solvent was removed in a rotary evaporator to yield a grey solid, which was filtered off and washed with diethyl ether. Again, the red solution was evaporated with a rotary evaporator giving a brown powder used without further purification (0.38 g, 85%). ^{1}H-NMR (300 MHz, $CDCl_3$) δ = 7.31 (d, *J* = 8.62 Hz, 4H, phenyl), 6.88 (s, 2H, thiophene), 6.66 (d, *J* = 8.62 Hz, 4H, phenyl), 2.83 (t, *J* = 7.43 Hz, 4H, cyclopentene), 2.06 (qt, *J* = 7.38 Hz, 2H, cyclopentene), 1.97 (s, 6H, CH_3). HRMS *m/z* 443.1590 ($[M + H]^+$, calculated for $C_{27}H_{27}N_2S_2$, 443.1616).

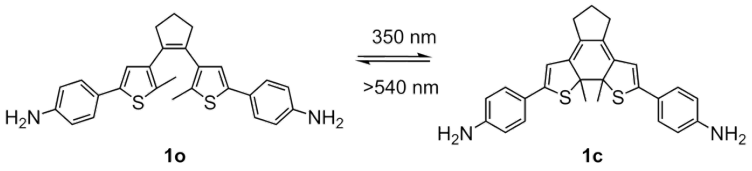

Scheme 2. Photoswitching behaviour of **1**.

Closed-ring isomer of 1o (1c). 1o (0.7 mM) in MeOH was placed in a beaker with stirring and then subjected to UV irradiation (350 nm) in a photoreactor for approximately 15 min. A dark purple solution was obtained, which was rotary evaporated to afford a dark purple solid, and it was used without any purification and isolation.

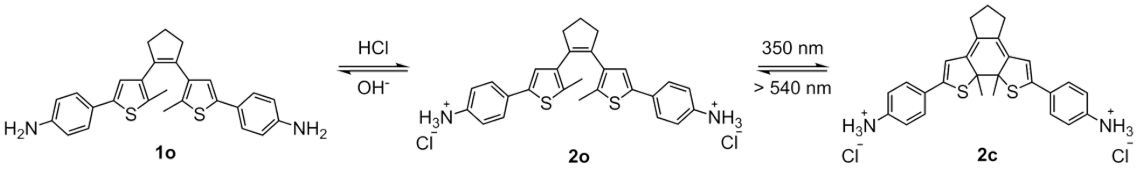

Scheme 3. Synthetic route and photoswitching behaviour of **2**.

1,2-Bis[2-methyl-5-(4-aminophenyl)-3-thienyl]cyclopentene hydrochloride (2o). To a EtOH/H_2O solution (2:1, 68 mL) of **1o** (12.30 mg, 0.028 mmol), HCl 6 M (18 µL, 0.108 mmol) was added. Then, the obtained grey-yellow solution was precipitated with diethyl ether, affording a grey solid, which was used without purification. IR (ν_{max}/cm^{-1}): 3442(vs, br), 2911(s), 2839(s), 2583(m), 1616(m), 1540(m), 1509(s), 1473(vw), 1437(w), 1311(vw), 1288(vw), 1210(w), 1117(w), 1016(vw), 948(vw), 820(m), 755(vw), 678(vw), 659(vw), 634(w), 558(vw), 487(m), 473(w), 429(w).

Closed-ring isomer of 2o (2c). 1o (12.30 mg, 0.028 mmol) was dissolved in EtOH/H_2O (2:1, 68 mL) and HCl 6M (18 µL, 0.108 mmol) was added. Then, the solution was placed in a beaker with stirring and then subjected to UV irradiation (350 nm) in a photoreactor for approximately 10 min. A dark violet solution was obtained and it was used without any purification nor isolation. IR (ν_{max}/cm^{-1}): 3399(m, br), 3178(m), 2920(vs), 2851(vs), 2567(s), 1604(s), 1560(m), 1509(s), 1471(s), 1425(s), 1349(m), 1315(s), 1269(s), 1177(vs), 1163(vs), 1076(m), 1059(m), 1019(w), 997(s), 921(w), 894(m), 821(m), 743(vw), 669(vw), 632(vw), 542(w), 487(w).

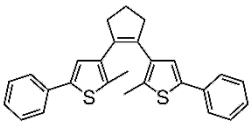

Scheme 4. Molecular structure of **3-H**.

Closed ring isomer of 3-Ho (3-Hc). 3-Ho (0.20 g, 0.485 mmol) was dissolved in hexane (100 mL) and then subjected to UV irradiation (308 nm) in a photoreactor for 1 h and 15 minutes giving a dark purple solution. The compound was crystallised by slow evaporation in acetonitrile yielding a mixture of dark purple and colourless crystals as minor impurities, which were removed manually. ^{1}H-NMR (300 MHz, $CDCl_3$) δ = 7.52 (t, *J* = 7.76 Hz, 4H, phenyl), 7.36 (t, *J* = 7.06 Hz, 4H, phenyl), 7.32 (t, *J* = 6.60 Hz, 2H, phenyl), 6.42 (s, 2H, thiophene), 2.50 (t, *J* = 7.34 Hz, 4H, cyclopentene), 2.03 (s, 6H, CH_3), 1.92 (qt, *J* = 7.29 Hz, 2H, cyclopentene).

1.2 Molecular functionalisation

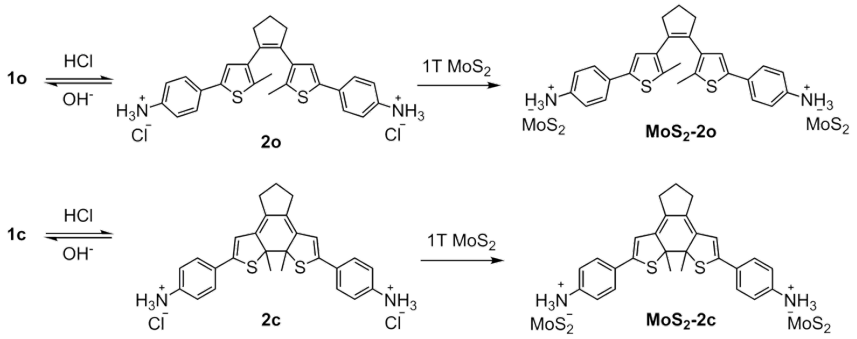

Scheme 5. Electrostatic functionalisation of **MoS_2-2**.

MoS_2-2o. To a solution of **1o** (43.97 mg, 0.1 mmol) in EtOH/H_2O (2:1, 180 mL), HCl 6M (64.4 µL) was added to afford **2o** with the resulting colour change from salmon to grey-yellow ($pH_{theo} \approx 2.8$). Then, an aqueous solution of ce-MoS_2 (0.1 mmol) was added dropwise under an inert atmosphere. The reaction mixture was stirred for 30 minutes yielding a black suspension. The suspension was centrifuged, and a black solid was collected. Then, it was washed with a mixture of EtOH/H_2O (2:1), and then dried under vacuum in the darkness.

MoS_2-2c. **1o** (43.97 mg, 0.1 mmol) was dissolved in EtOH/H_2O (1:1, 244 mL) and then, HCl 6M (64.4 µL) was added. Next, the reaction mixture was subjected to UV irradiation (350 nm) in a photoreactor for 10 min to afford **2c**. An aqueous solution of ce-MoS_2 (0.1 mmol) was added dropwise under an inert atmosphere. The reaction mixture was stirred for 30 minutes yielding a black suspension. The suspension was centrifuged. The remaining solid was washed with a mixture of EtOH/H_2O (2:1), then dried under vacuum.

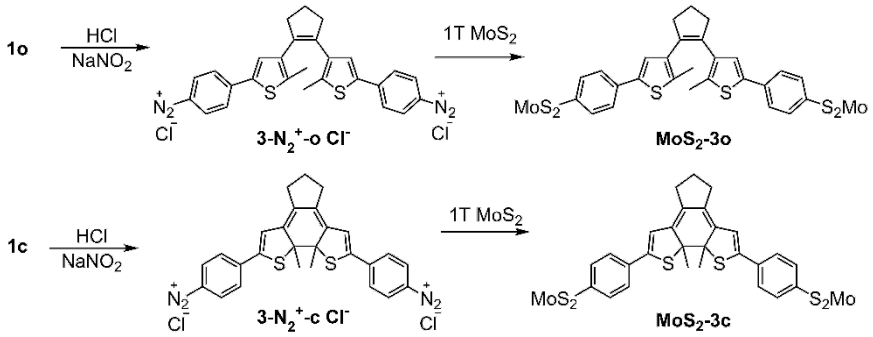

Scheme 6. Covalent functionalisation of **MoS_2-3**.

MoS_2-3o. 1 (12.30 mg, 0.028 mmol) was suspended in water under an argon atmosphere. Subsequently, sodium nitrite (5.77 mg, 0.084 mmol) and HCl 6 M (511 µL) were added at 0 °C, and the resultant mixture was stirred for 1 h. Then, an aqueous suspension of ce-MoS_2 flakes (0.28 mmol) was added and stirred at room temperature for 24 h. After, the solid was filtered, washed with water, DMSO, and MeOH and dried under vacuum for 14 h in the darkness, at least.

MoS_2-3c. A solution of **1o** (12.30 mg, 0.028 mmol) in 40 mL of MeOH was subjected to UV irradiation (350 nm) in a photoreactor during 15 min under vigorous magnetic stirring. The resulting dark purple solution was rotary evaporated to yield a purple solid (**1c**). Finally, the procedure described for the synthesis of **MoS_2-3o** was followed.

Physical mixture

ce-MoS_2+3-Ho. The physical mixture of ce-MoS_2 with **3-Ho** was prepared by grinding 7.2 mg of ce-MoS_2 flakes and 2.3 mg of **3-Ho** in a mortar (**3-Ho**/MoS_2 molar ratio of ≈0.1).

1.3 Characterisation

Nuclear magnetic resonance spectroscopy (RMN). ^{1}H-RMN data were recorded at room temperature on a Bruker DPX300 spectrophotometer. Chemical shifts are reported in ppm, and they are referenced to $CDCl_3$.

Electrospray mass spectroscopy (ESI-MS). High-resolution ESI-MS in methanol solution were obtained on an AB SCIEX TripleTOF™ 5600 LC/MS/MS System.

Liquid UV/Vis spectroscopy. Spectra were recorded using Hellma quartz cuvettes and on a Jasco V-670 spectrophotometer and powder UV/Vis spectra were recorded using the PIN-757 adaptor.

Infrared spectroscopy. Spectra (4000–400 cm^{-1}) were recorded on a Nicolet 5700 spectrophotometer as KBr pellets. All samples were measured as KBr pellets, and transmittance intensities were scaled for comparison purposes.

Raman spectroscopy. Spectra were recorded with a Horiba-LabRam HR Evolution Spectrometer in ambient conditions. The measurements were performed with 8 mW (532 nm), 17 mW (633 nm) and 26 mW (785 nm) excitation power. A spot size of ~2μm diameter was used for all experiments. The spectrophotometer is equipped with laser filters that allow to diminish the laser beam power by selecting 0.1, 0.5, 1, 5, 10, 25, 50 100% laser power.

X-ray powder diffraction (XRPD). XRPD patterns were performed on a Panalytical Empyrean X-ray diffractometer by using Cu Kα radiation (λ= 1.5406 Å), in which the X-ray tube was operated at 45 kV and 40 mA ranging from 2 to 90°. The XRPD data was background corrected with the HighScore Plus software.

Thermogravimetric analysis (TGA). Experiments were conducted using a TA Instrument TGA550 in the 25–850 °C range under a 10 °C min^{-1} scan rate and N_2 flow of 100 mL min^{-1}.

X-ray photoelectron spectroscopy (XPS). XPS spectra were analysed using a Thermo Scientific K-alpha X-ray photoelectron spectrometer, using a monochromatic Al Kα radiation (1486.6 eV) at a pressure of $4 \cdot 10^{-9}$ mBar. XPS data were analysed with Avantage software, where the binding energy of the C 1s at 284.8 eV was used as reference to adjust the position of the other peaks.

1.4 Photoswitching studies

Photoreactor experiments. 1–**3-H** diarylethene molecules were irradiated inside a commercial photoreactor (LuzChem LZC-4V), with 14 UVB (308 nm) lamps, 14 UVA FL8BL-B (350 nm) lamps and 12 Sylvania Cool White F8T5 (visible) lamps with LuzChem orange filters (> 540 nm).

Raman experiments. MoS_2-2 and **MoS_2-3** were deposited onto clean SiO_2 (285 nm)/Si substrates by drop-casting of their suspensions. Raman spectra were collected at 532 nm with 1% laser power. To induce photoswitching reactions, samples were irradiated with Raman lasers at different wavelengths (532 and 633 nm) with 5% laser power at different times. Next, Raman spectra were recorded on the same spot area with the Raman spectrophotometer at 532 nm with 1% laser power. Irradiating the samples with lower laser powers led to very noisy measurements, and at higher powers resulted in MoS_2 oxidation and sample burnings.

2 Ce-MoS_2 characterisation

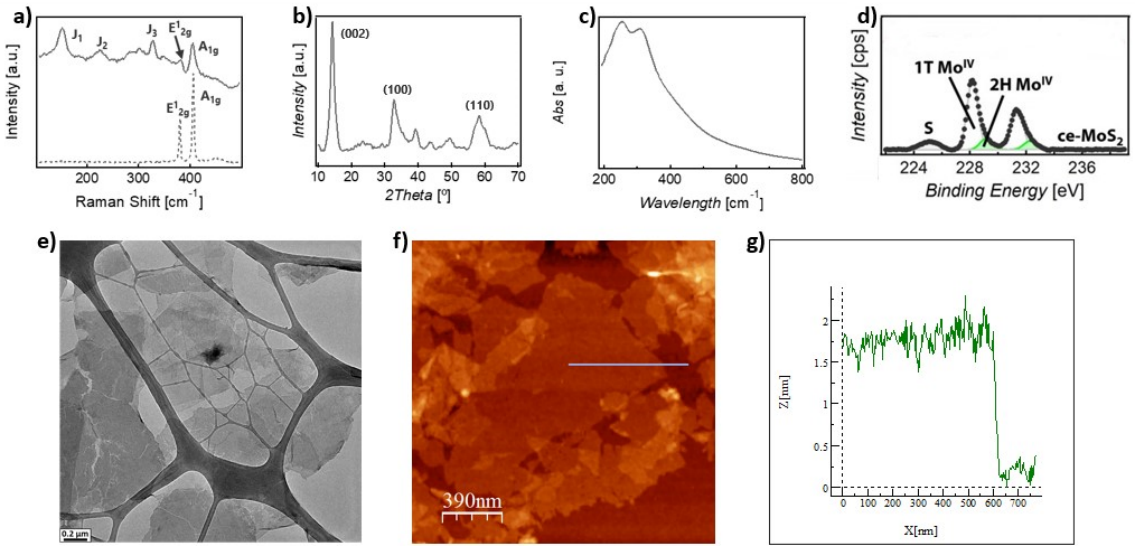

Fig. S1 Raman spectra of ce-MoS_2 (top) and commercial 2H-MoS_2 (down) measured at 532 nm excitation wavelength, b) PXRD pattern of ce-MoS_2, c) UV/Vis absorption spectrum of ce-MoS_2 in water d) XPS spectrum of ce-MoS_2, e) TEM image of ce-MoS_2 flakes, f) AFM topographic image of ce-MoS_2 flakes, g) Height profile of a ce-MoS_2 flake shown in f).

3 TEM characterisation

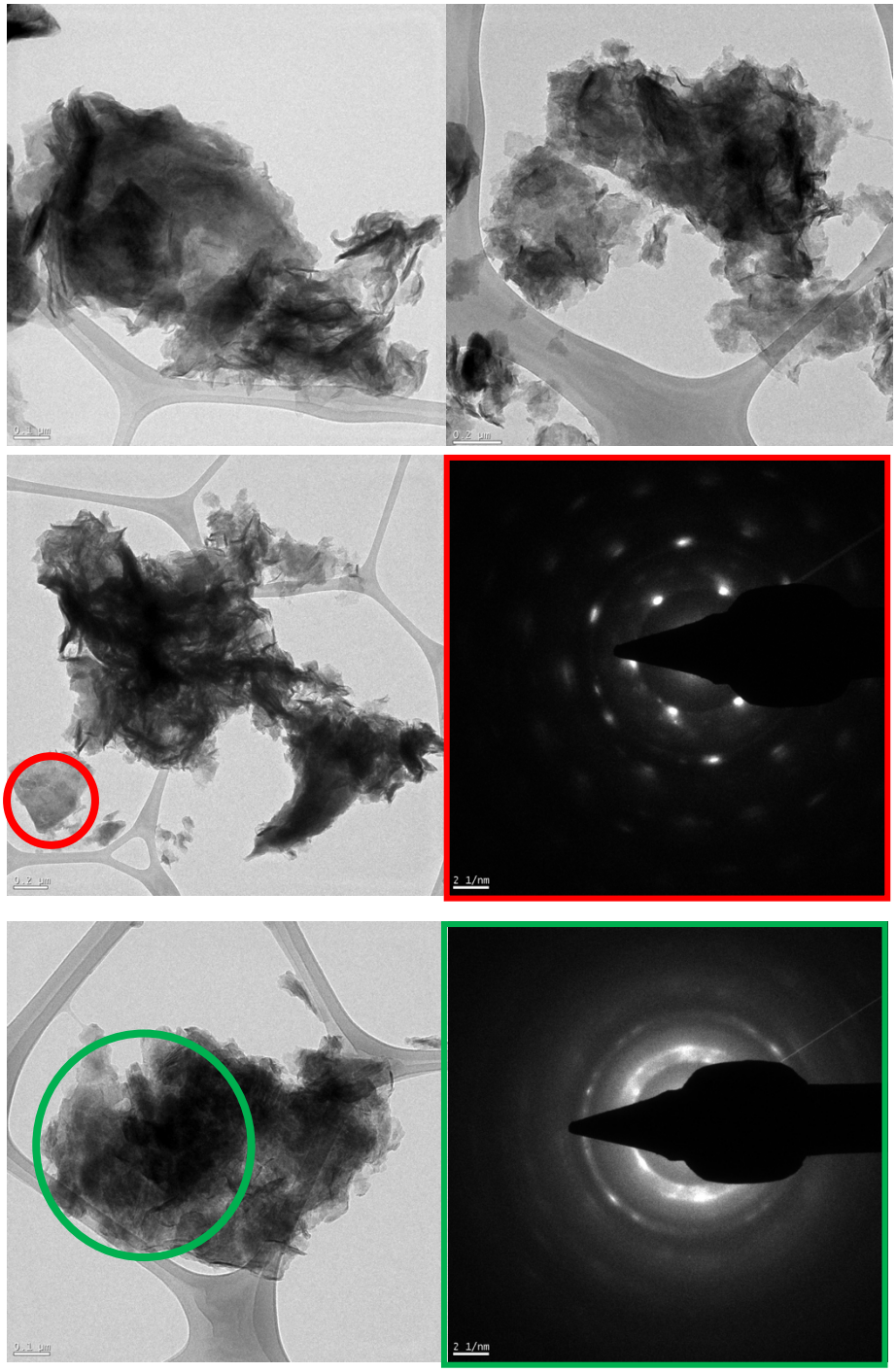

Fig. S2. Top: TEM images of **MoS_2-3o** (left) and **MoS_2-3c** (right). Middle: TEM image of **MoS_2-3o** and SAED image of a non-wrinkled region circled in red. Bottom: TEM image of **MoS_2-3c** and SAED image of a wrinkled region circled in green.

4 IR spectroscopy

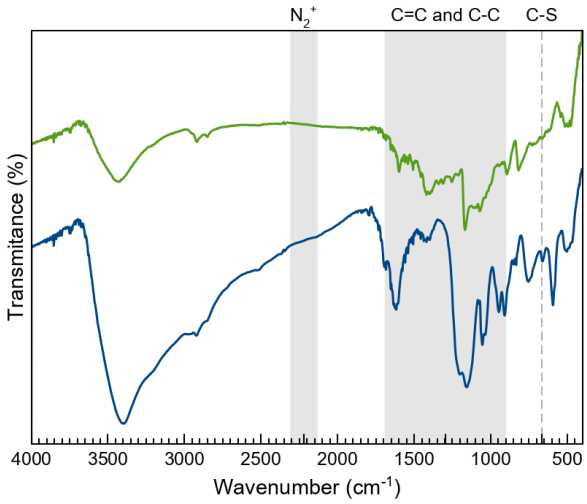

Fig. S3. FTIR spectra of **MoS_2-2c** (green) and **MoS_2-3c** (blue).

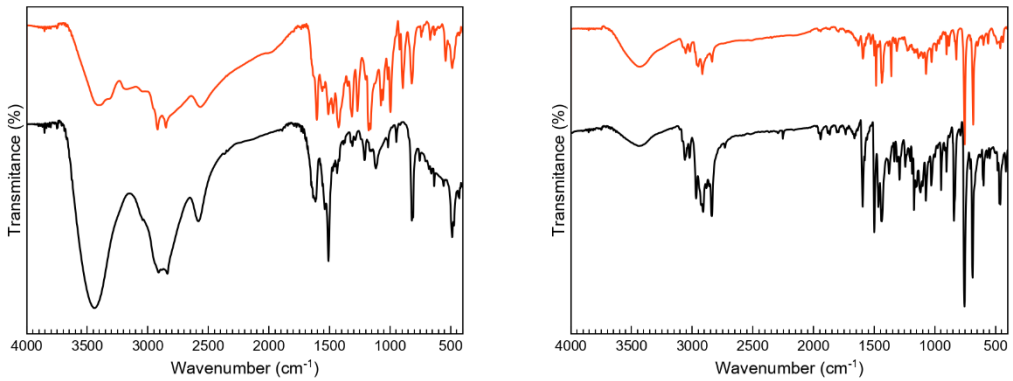

Fig. S4. FTIR spectra for the open (black) and closed (orange) forms of **2** (left) and **3-H** (right).

5 XPS spectroscopy

Table S1. XPS values observed in **1o**, **MoS_2-2** and **MoS_2-3**.

Mo peaks (eV)	S peaks (eV)	N peaks (eV)
1o		
	~163.7 S^{2-} $2p_{3/2}$ (S–C)	~399.4 N 1s (NH_2)
	~164.9 S^{2-} $2p_{1/2}$ (S–C)	
MoS_2-2o and MoS_2-2c		
~228.2 Mo^{IV} $3d_{5/2}$ (1T MoS_2)	~161.1 S^{2-} $2p_{3/2}$ (1T MoS_2)	~399.4 N 1s (NH_2)
~228.9 Mo^{IV} $3d_{5/2}$ (2H MoS_2)	~161.8 S^{2-} $2p_{3/2}$ (2H MoS_2)	
~229.9 Mo^{IV} $3d_{5/2}$ (MoO_2)	~162.2 S^{2-} $2p_{1/2}$ (1T MoS_2)	
~231.4 Mo^{IV} $3d_{3/2}$ (1T MoS_2)	~162.9 S^{2-} $2p_{1/2}$ (2H MoS_2)	
~232.1 Mo^{IV} $3d_{3/2}$ (2H MoS_2)	~163.7 S^{2-} $2p_{3/2}$ (S-C)	
~232.5 Mo^{VI} $3d_{5/2}$	~164.9 S^{2-} $2p_{1/2}$ (S-C)	
~233.0 Mo^{IV} $3d_{3/2}$ (MoO_2)	~226.1 S^{2-} 2s	
~235.7 Mo^{VI} $3d_{3/2}$		
MoS_2-3o and MoS_2-3c		
~228.8 Mo^{IV} $3d_{5/2}$ (2H MoS_2)	~161.2 S^{-} $2p_{3/2}$	
~229.9 Mo^{IV} $3d_{5/2}$ (2H MoO_2)	~161.8 S^{2-} $2p_{3/2}$ (2H MoS_2)	
~231.0 Mo^{V} $3d_{5/2}$	~162.1 S^{-} $2p_{1/2}$	
~232.0 Mo^{IV} $3d_{3/2}$ (2H MoS_2)	~162.9 S^{2-} $2p_{1/2}$ (2H MoS_2)	
~233.0 Mo^{IV} $3d_{3/2}$ (2H MoO_2)	~163.7 S^{2-} $2p_{3/2}$ (S–C)	
~234.3 Mo^{V} $3d_{3/2}$	~164.9 S^{2-} $2p_{1/2}$ (S–C)	
	~226.2 S^{2-} 2s	

5 Molecular representation of 3

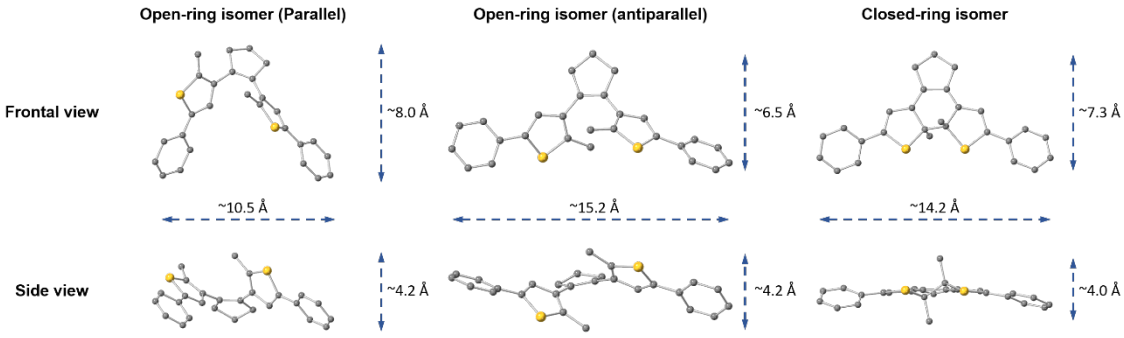

Fig. S5. Frontal- and side-views of the open isomer in the parallel (not suitable for photoswitching behavior) and antiparallel configurations, and the closed isomer of **3-H** in crystals.

6 Raman spectroscopy

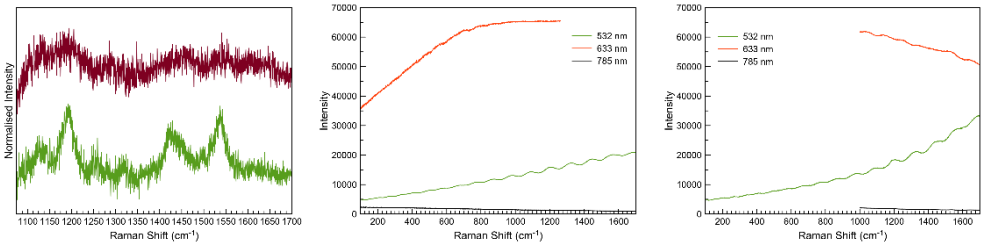

Fig. S6. Normalised Raman spectra of **2o** (red) and **2c** (green) as solid at 785 nm wavelength (left). Normalised Raman spectra of **2o** (middle) and **2c** (right) as solids at 532 (green), 633 (orange) and 785 nm (black) wavelength**.**

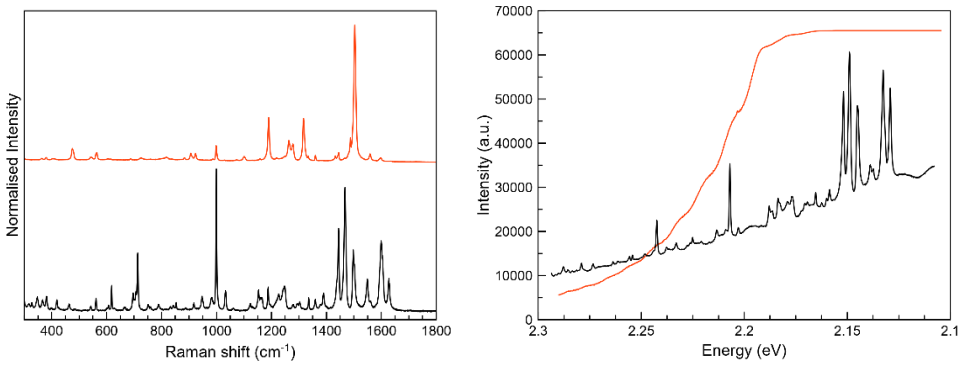

Fig. S7. Normalised Raman spectra of **3-Ho** (black) and **3-Hc** (orange) as solid at 785 nm wavelength (left). Photoluminescence spectra of **3-Ho** (black) and **3-Hc** (red) as solids at 532 nm (right).

7 TGA analysis

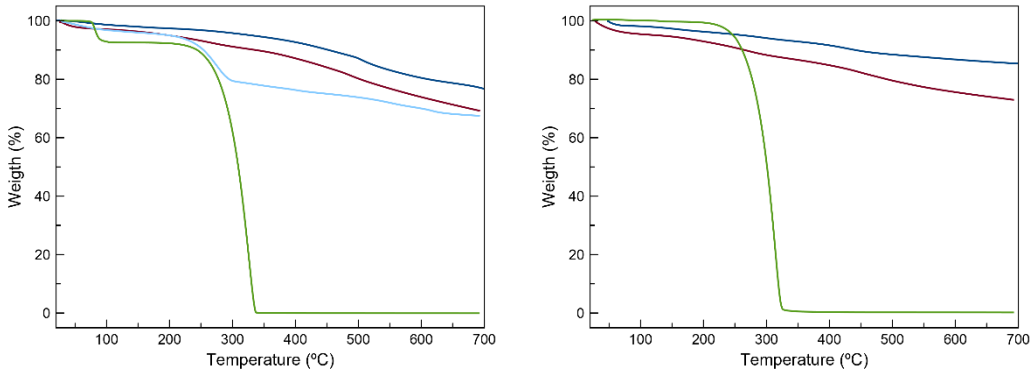

Fig. S8. TGA plots of **3-H** (green), physical mixture **ce-MoS_2+3-H** (light blue), **MoS_2-3** (red) and **MoS_2-2** (dark blue) for open (left) and closed (right) isomers.

8 Photoswitching behaviour

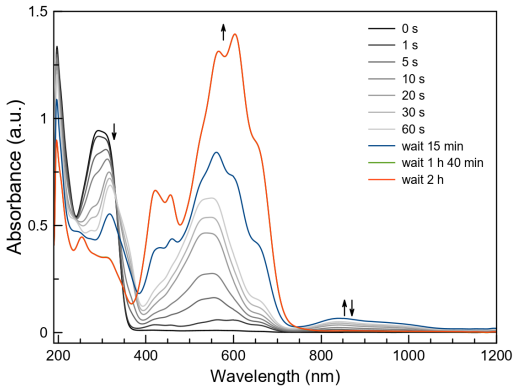

Fig. S9. UV/Vis absorption spectra of **2o** in EtOH/H_2O (70%) at different irradiation times with 350 nm lamps (grey gradient). Kinetics of protonation after irradiation at different times (blue, green and red lines).

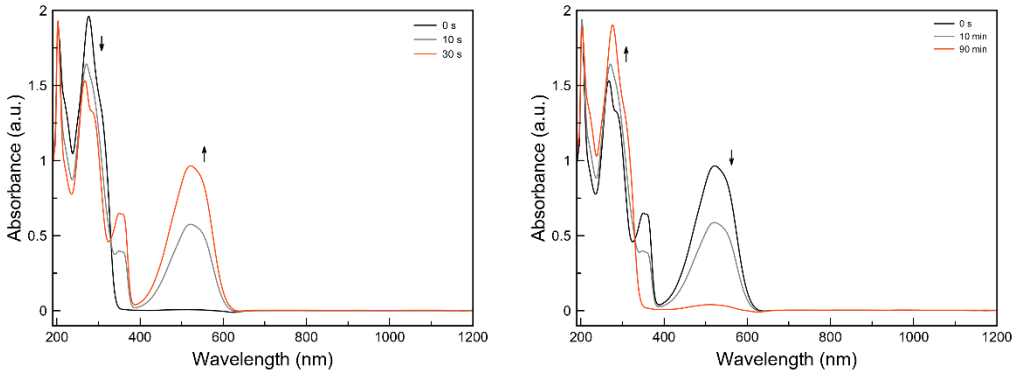

Fig. S10. UV/Vis absorption spectra of **3-H** in MeOH at different irradiation times with 308 nm (left) and visible lamps with >540 nm orange filters (right).

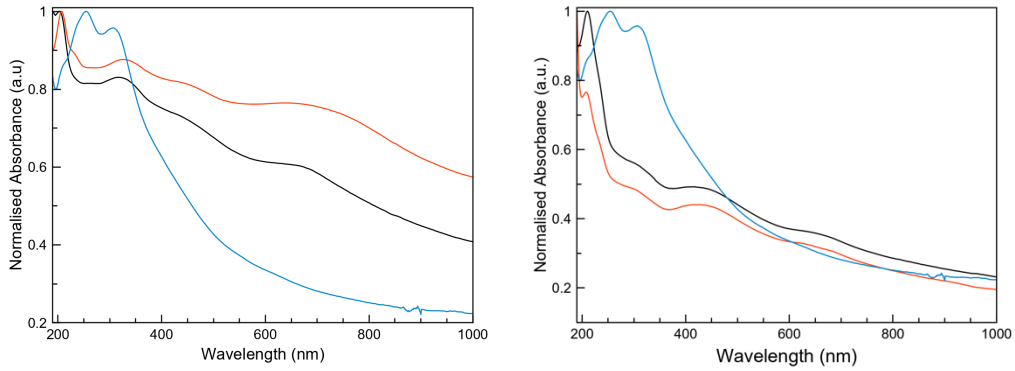

Fig. S11. UV/Vis absorption spectra of aqueous suspensions of **MoS_2-2** (left) and **MoS_2-3** (right) for the open (black) and closed (red) isomers and ce-MoS_2 (blue).

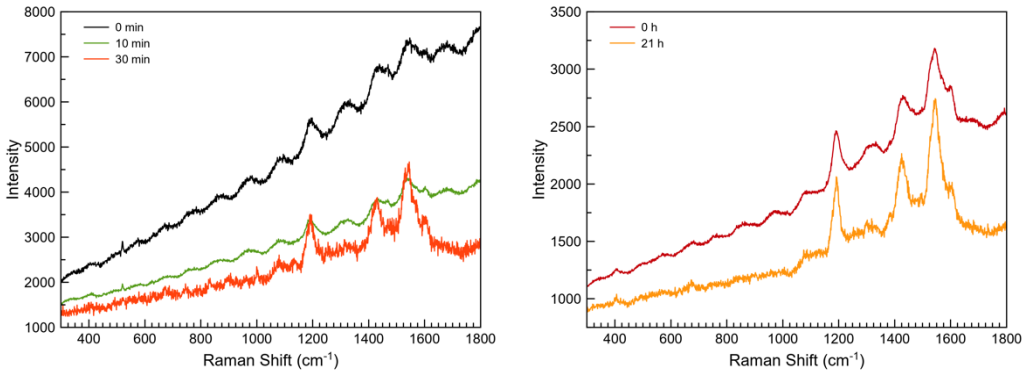

Fig. S12. Raman spectra of **2o** deposited onto a SiO_2/Si substrate by drop casting and measured at 532 nm excitation wavelength before (black) and after irradiation experiments in a photoreactor with 350 nm lamps (left). Raman spectra of **2c** deposited onto a SiO_2/Si substrate by drop casting and measured at 532 nm excitation wavelength before (red) and after (orange) irradiation experiments in a photoreactor with visible lamps with >540 nm orange filters (right).

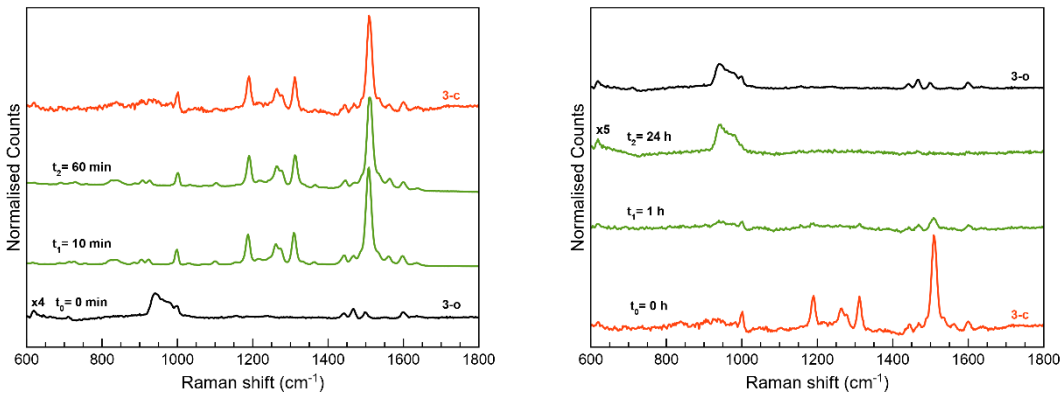

Fig. S13. Raman spectra of **3-Ho** (left) and **3-Hc** (right) deposited onto a SiO_2/Si substrate by drop casting and measured at 785 nm excitation wavelength before and after irradiation experiments in a photoreactor. The spectra were baseline corrected and some spectra were magnified for comparison purposes. A partial degradation upon the closed-ring aperture cannot be discarded because of the weak signals registered after the irradiation, even though the peak intensity of **3-H** is substantially low when drop-casted on the SiO_2 substrate.

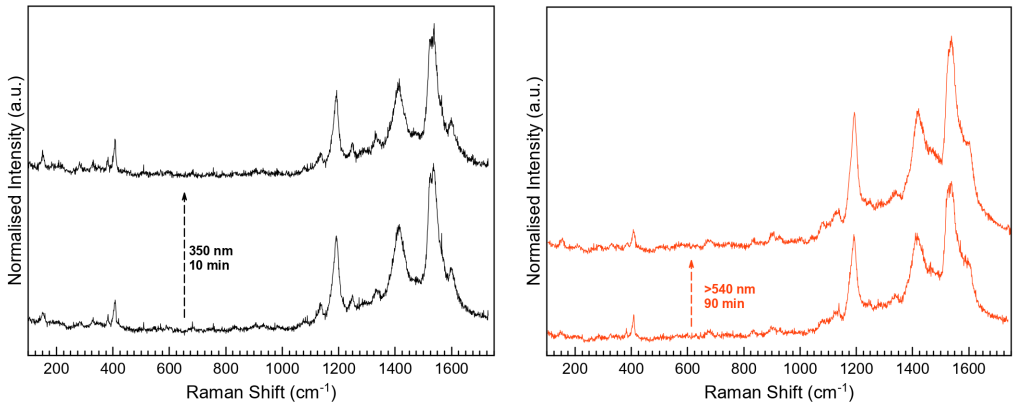

Fig. S14. Raman spectra at 532 nm of **MoS_2-2** deposited onto a SiO_2/Si substrate by drop casting and irradiated into a photoreactor at 350 nm (**MoS_2-2o**, left) and >540 nm (**MoS_2-2c**, right) for 90 minutes.

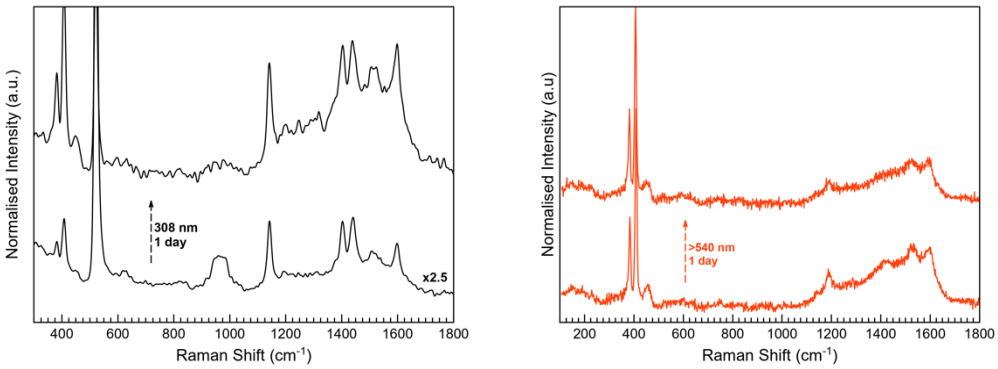

Fig. S15. Raman spectra at 532 nm of **MoS_2-3** deposited onto a SiO_2/Si substrate and irradiated into a photoreactor at 308 nm (**MoS_2-3o**, left) and >540 nm (**MoS_2-3c**, right) for 1 day.

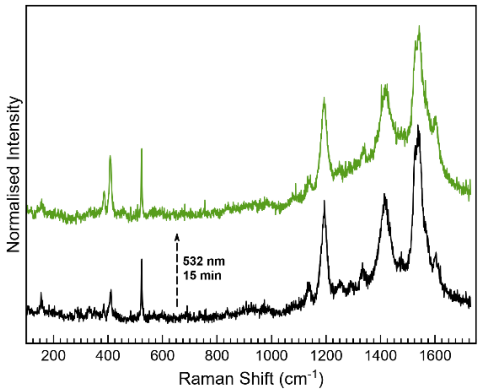

Fig. S16. Raman spectra at 532 nm for **MoS_2-2o** deposited onto SiO_2/Si substrates (black) by drop casting and the resulting irradiation using a 532 nm laser at 5% power (green).

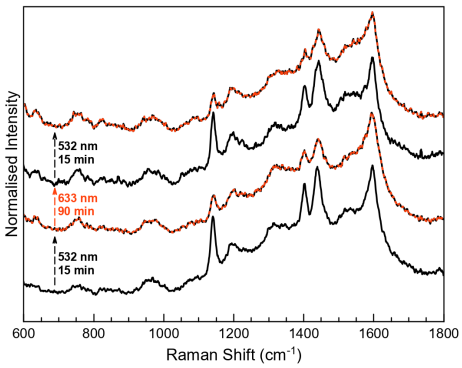

Fig. S17. Raman spectra for the irradiated **MoS_2-3o** sample deposited on SiO_2/Si by drop casting and measured with a 532 nm excitation laser with 1% laser power. The open-ring isomer, the closed-ring isomer and a mixture of open-ring and closed-ring isomers are represented as black, red and black-red lines, respectively.

9 DFT and TDDFT calculations

Geometries of the open and closed form of **3-H** were optimized by PM6 semiempirical methods and DFT type calculations through the Gaussian 09 package by using the PBEPBE functional,[3-5] the quadratic convergence approach.[6,7] For the last method, a 6-31G all-electron basis set proposed by Pople *et al.* was used for all atoms.[8-17] The energies and oscillator strengths for less energetic electronic transitions were calculated on both optimized geometries obtained for the two different methods through the time-dependent formalism applied on the PBEPBE functional and using the 6-31G basis set.[18-24] Both procedures provide similar results and validate the geometry optimization through semiempirical methods when the computational cost is excessive for larger models. Thus, this optimization on a model of the photo-switchable molecule anchored to a MoS_2 surface (Fig. S18) is carried by this less expensive strategy. The estimation of the features of the excited states, or the energies and type of electronic excitations, is a crucial step in this study. In order to find relatively accurate results in a suitable time, the optimized geometry is frozen and simplified by reducing the layer to only the MoS_2 unity directly linked to the organic molecule. In this way, electronic effects are kept, but we should proceed with caution because they can be magnified (Fig. S18). However, for a semiquantitative analysis, this procedure can be successful enough. The TD-DFT calculations for this last model were done using a LanL2DZ electron-valence basis set and effective core potential for the molybdenum atoms.[25-28] Orbitals and spin densities maps were plotted through the Gabedit 2.5 software.[29]

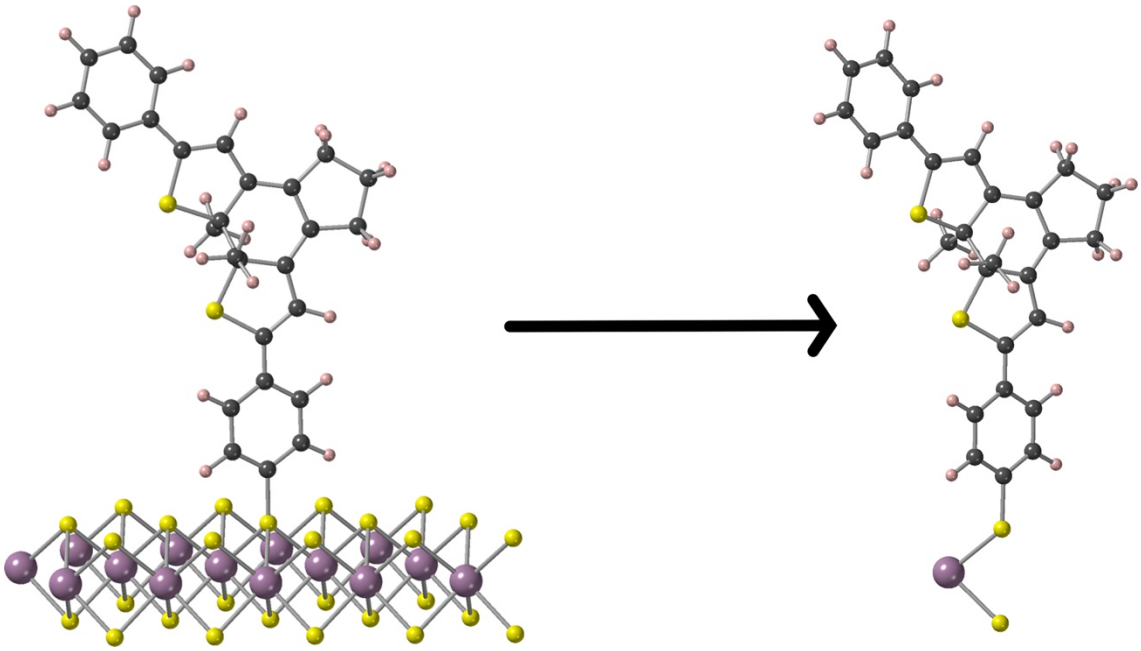

Fig. S18. Molecular model used to simulate **MoS_2-3o** and **MoS_2-3c** composites (left) and the subsequent simplification (right) applied to carry TD-DFT calculations.

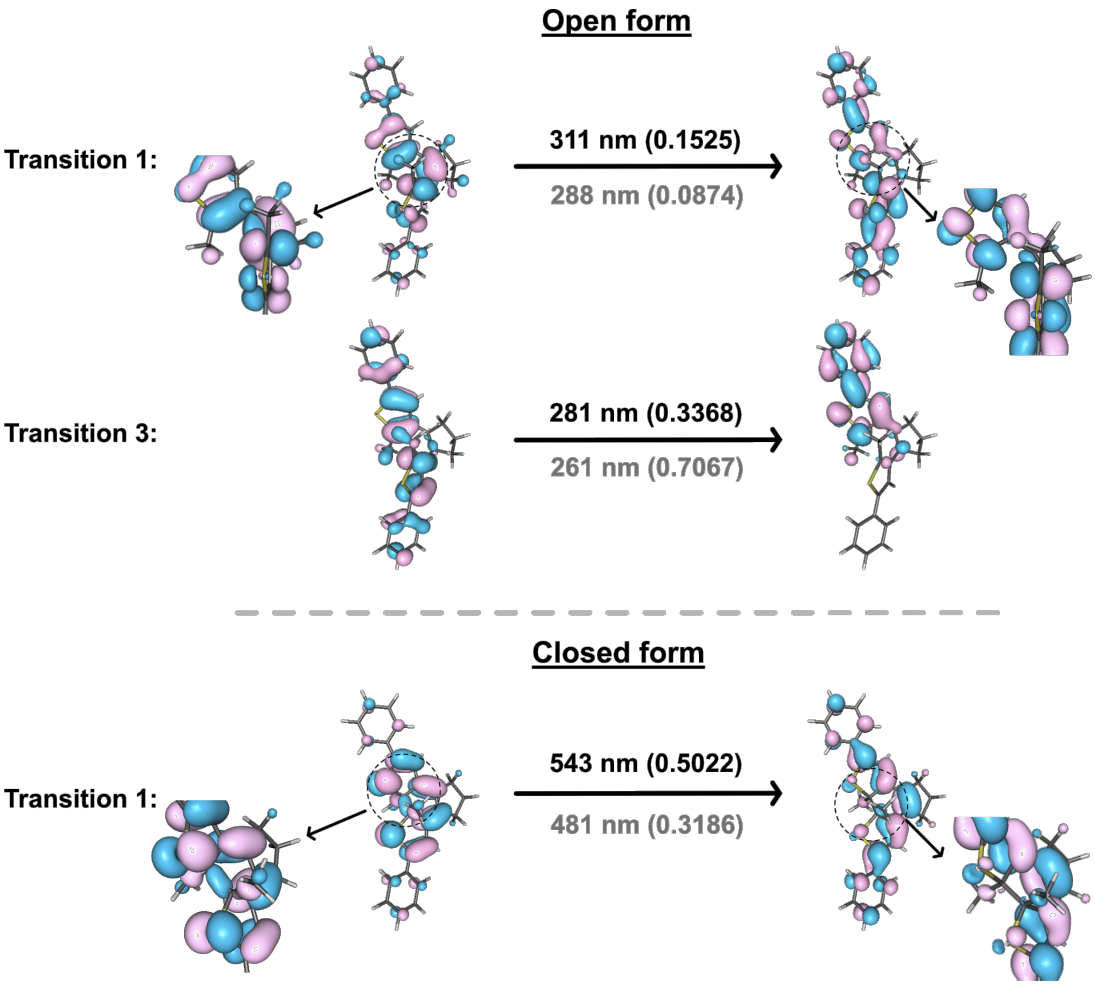

Fig. S19. Perspective views of the natural transition orbitals (NTOs) involved in some significant theoretical electronic excitations of the open and closed forms of the free organic molecule (**3-H**). The isodensity surfaces correspond to a cut-off value of 0.05 e bohr^{-3}. Electrons are promoted from the orbital at the left side to the other one at the right side. Oscillator strengths are given in parentheses. Results on DFT and PM6 optimized geometries appear in black and grey colours.

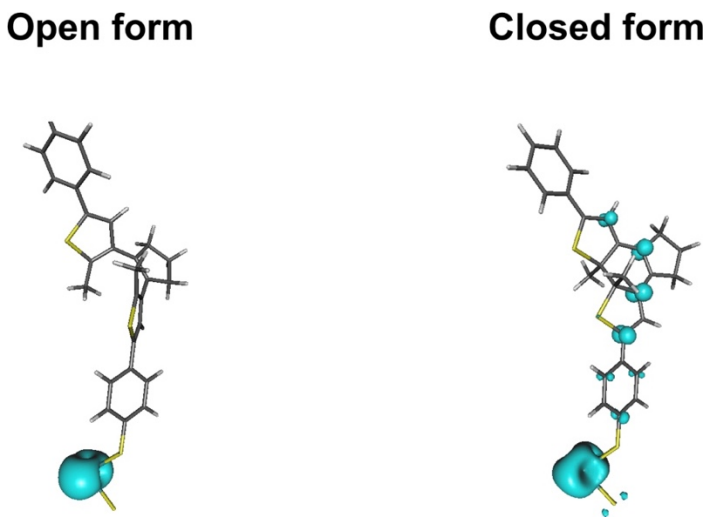

Fig. S20. Perspective views of the spin density distribution for the open and closed forms of the organic molecule anchored to the MoS_2. The isodensity surfaces correspond to a cut-off value of 0.005 e bohr^{-3}.

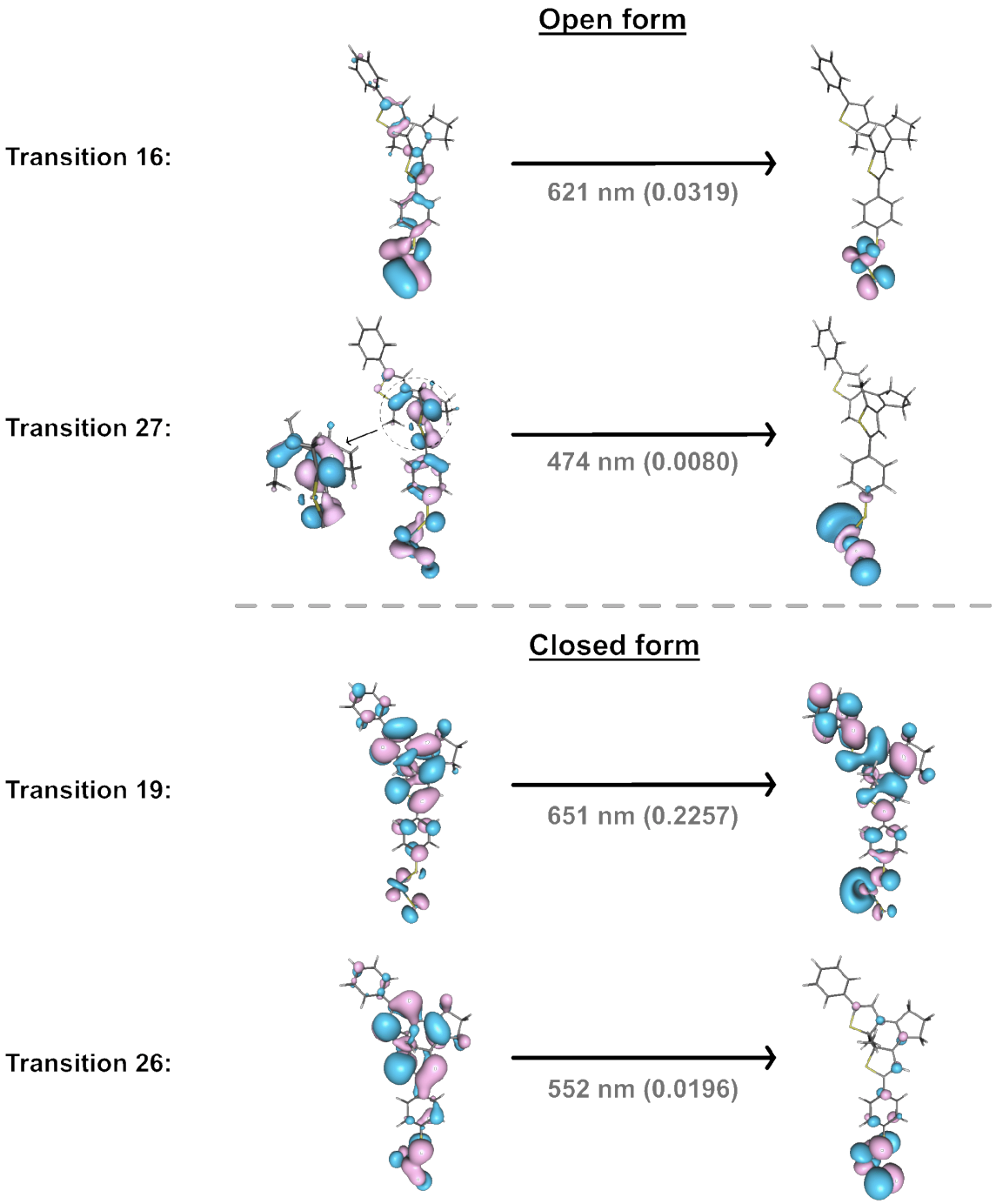

Fig. S21. Perspective views of the natural transition orbitals (NTOs) involved in some significant theoretical electronic excitations of the open and closed forms of the organic molecule anchored to a MoS_2 layer. The isodensity surfaces correspond to a cut-off value of 0.05 e bohr^{-3}. Electrons are promoted from the orbital at the left side to the other one at the right side. Oscillator strengths are given in parentheses. Results on PM6 optimized geometries appear in black and grey colours.

References

1 L. N. Lucas, J. J. D. De Jong, J. H. Van Esch, R. M. Kellogg and B. L. Feringa, *European J. Org. Chem.*, 2003, 155–166.

2 M. Morant-Giner, R. Sanchis-Gual, J. Romero, A. Alberola, L. García-Cruz, S. Agouram, M. Galbiati, N. M. Padial, J. C. Waerenborgh, C. Martí-Gastaldo, S. Tatay, A. Forment-Aliaga and E. Coronado, *Adv. Funct. Mater.*, 2018, **28**, 1706125.

3 J. J. P. Stewart, *J. Mol. Model.*, 2007, **13**,1173-213.

4 J. P. Perdew, K. Burke, and M. Ernzerhof, *Phys. Rev. Lett.*, 1996, **77,** 3865-3868.

5 J. P. Perdew, K. Burke, and M. Ernzerhof, *Phys. Rev. Lett.*, 1997, **78**, 1396.

6 G. B. Bacskay, *Chem. Phys.*, 1981, **61**, 385-404.

7 M. J. Frisch, G. W. Trucks, H. B. Schlegel, G. E. Scuseria, M. A. Robb, J. R. Cheeseman, G. Scalmani, V. Barone, B. Mennucci, G. A. Petersson, H. Nakatsuji, M. Caricato, X. Li, H. P. Hratchian, A. F. Izmaylov, J. Bloino, G. Zheng, J. L. Sonnenberg, M. Hada, M. Ehara, K. Toyota, R. Fukuda, J. Hasegawa, M. Ishida, T. Nakajima, Y. Honda, O. Kitao, H. Nakai, T. Vreven, J. A. Montgomery Jr., J. E. Peralta, F. Ogliaro, M. Bearpark, J. J. Heyd, E. Brothers, K. N. Kudin, V. N. Staroverov, R. Kobayashi, J. Normand, K. Raghavachari, A. Rendell, J. C. Burant, S. S. Iyengar, J. Tomasi, M. Cossi, N. Rega, J. M. Millam, M. Klene, J. E. Knox, J. B. Cross, V. Bakken, C. Adamo, J. Jaramillo, R. Gomperts, R. E. Stratmann, O. Yazyev, A. J. Austin, R. Cammi, C. Pomelli, J. W. Ochterski, R. L. Martin, K. Morokuma, V. G. Zakrzewski, G. A. Voth, P. Salvador, J. J. Dannenberg, S. Dapprich, A. D. Daniels, Ö. Farkas, J. B. Foresman, J. V Ortiz, J. Cioslowski, D. J. Fox, *Gaussian 09,* Gaussian, Inc., Wallingford CT, **2009**.

8 R. Ditchfield, W. J. Hehre, and J. A. Pople, *J. Chem. Phys.*, 1971, **54**, 724.

9 W. J. Hehre, R. Ditchfield, and J. A. Pople, *J. Chem. Phys.*, 1972, **56**, 2257.

10 P. C. Hariharan and J. A. Pople, "Influence of polarization functions on molecular-orbital hydrogenation energies," *Theor. Chem. Acc.*, 1973, **28,** 213-22.

11 P. C. Hariharan and J. A. Pople, *Mol. Phys.*,1974, **27** 209-214.

12 M. S. Gordon, *Chem. Phys. Lett.*, 1980, **76,** 163-168.

13 M. M. Francl, W. J. Pietro, W. J. Hehre, J. S. Binkley, D. J. DeFrees, J. A. Pople, and M. S. Gordon, *J. Chem. Phys.*, 1982, **77**, 3654-3665.

14 R. C. Binning Jr. and L. A. Curtiss, *J. Comp. Chem.*,1990, **11**, 1206-1216.

15 J.-P. Blaudeau, M. P. McGrath, L. A. Curtiss, and L. Radom, *J. Chem. Phys.*,1997, **107,** 5016-5021.

16 V. A. Rassolov, J. A. Pople, M. A. Ratner, and T. L. Windus, *J. Chem. Phys.*, 1998, **109**, 1223-1229.

17 V. A. Rassolov, M. A. Ratner, J. A. Pople, P. C. Redfern, and L. A. Curtiss, *J. Comp. Chem.*, 2001, **22,** 976-984.

18 R. Bauernschmitt and R. Ahlrichs, *Chem. Phys. Lett.*, 1996, **256**, 454-464.

19 M. E. Casida, C. Jamorski, K. C. Casida, and D. R. Salahub, *J. Chem. Phys.*, 1998, **108**, 4439-4349.

20 R. E. Stratmann, G. E. Scuseria, and M. J. Frisch, *J. Chem. Phys.*,1998, **109,** 8218-8124.

21 C. Van Caillie and R. D. Amos, *Chem. Phys. Lett.*, 1999, **308**, 249-255.

22 C. Van Caillie and R. D. Amos, *Chem. Phys. Lett.*, 2000, **317**, 159-164.

23 F. Furche and R. Ahlrichs, *J. Chem. Phys.*, 2002, **117,** 7433-7447.

24 G. Scalmani, M. J. Frisch, B. Mennucci, J. Tomasi, R. Cammi, and V. Barone, *J. Chem. Phys.*, 2006, **124,** 094107: 1-15.

25 T. H. Dunning Jr. and P. J. Hay, in *Modern Theoretical Chemistry*, Ed. H. F. Schaefer III, Vol. 3 (Plenum, New York, 1977) 1-28.

26 P. J. Hay and W. R. Wadt, *J. Chem. Phys.*, 1985, **82,** 270-283.

27 W. R. Wadt and P. J. Hay, "Ab initio effective core potentials for molecular calculations – potentials for main group elements Na to Bi," *J. Chem. Phys.*, 1985, **82,** 284-298.

28 P. J. Hay and W. R. Wadt, *J. Chem. Phys.*, 1985, **82,** 299-310.

29 A.R. Allouche, *J. Comput. Chem*., 2011, **32**, 174-182.